Tau tubulin kinase is required for spermatogenesis and development of motile cilia in planarian flatworms

Robert Alan Magley and Labib Rouhana*
Department of Biological Sciences, Wright State University, Dayton, OH 45435

ABSTRACT Cilia are microtubule-based structures that protrude from the apical surface of cells to mediate motility, transport, intracellular signaling, and environmental sensing. Tau tubulin kinases (TTBKs) destabilize microtubules by phosphorylating microtubule-associated proteins (MAPs) of the MAP2/Tau family, but also contribute to the assembly of primary cilia during embryogenesis. Expression of TTBKs is enriched in testicular tissue, but their relevance to reproductive processes is unknown. We identified six TTBK homologues in the genome of the planarian *Schmidtea mediterranea* (*Smed-TTBK-a, -b, -c, -d, -e,* and *-f*), all of which are preferentially expressed in testes. Inhibition of *TTBK* paralogues by RNA interference (RNAi) revealed a specific requirement for *Smed-TTBK-d* in postmeiotic regulation of spermatogenesis. Disrupting expression of *Smed-TTBK-d* results in loss of spermatozoa, but not spermatids. In the soma, *Smed-TTBK-d* RNAi impaired the function of multiciliated epidermal cells in propelling planarian movement, as well as the osmoregulatory function of protonephridia. Decreased density and structural defects of motile cilia were observed in the epidermis of *Smed-TTBK-d(RNAi)* by phase contrast, immunofluorescence, and transmission electron microscopy. Altogether, these results demonstrate that members of the TTBK family of proteins are postmeiotic regulators of sperm development and also contribute to the formation of motile cilia in the soma.

INTRODUCTION

Ciliopathies are a group of health disorders associated with mutations of factors involved in cilia formation and function. Included among these are variable pathologies of the kidney, liver, and retina, as well as brain dysgenesis, neurocognitive impairments, and infertility (Badano *et al.*, 2006; Lee and Gleeson, 2011; Waters and Beales, 2011; Reiter and Leroux, 2017). Members of the tau tubulin kinase (TTBK) subfamily of casein kinase proteins are associated with ciliopathies (Ikezu and Ikezu, 2014). As the name implies, TTBKs are able to directly phosphorylate tubulin (the main structural element of microtubules) and the microtubule-associated proteins (MAPs) MAP2 and Tau (Takahashi *et al.*, 1995; Tomizawa *et al.*, 2001; Sato *et al.*, 2006). Two members of the TTBK subfamily of proteins are encoded in the human genome. *TTBK1* is almost exclusively expressed in the CNS, and certain alleles are associated with late onset Alzheimer's disease (Vazquez-Higuera *et al.*, 2011; Yu *et al.*, 2011; Fagerberg *et al.*, 2014). *TTBK2* expression is detected broadly at the transcript level, but the protein is particularly abundant in the brain and testis (Bouskila *et al.*, 2011; Fagerberg *et al.*, 2014). Indeed, mutations in *TTBK2* are associated with spinocerebral ataxia type 11, which is characterized by progressive loss of coordination, difficulty walking, abnormal eye signs, peripheral neuropathy, and dystonia (Houlden *et al.*, 2007; Bauer *et al.*, 2010). The contributions of TTBK proteins in the development or function of the reproductive system remain unknown.

Given the shared components involved in the assembly of microtubules in somatic cell cilia and sperm flagella, it could be postulated that TTBK activity contributes to the process of

spermatogenesis. Second to levels of expression in neurons, for which functional relevance has been extensively established, the activity of mammalian *TTBK* paralogues is highest in male gonads (Sato *et al.*, 2006; Bouskila *et al.*, 2011; Fagerberg *et al.*, 2014; Papatheodorou *et al.*, 2018). However, functional studies in mice have not revealed a role for TTBK homologues in spermatogenesis. Humanized *TTBK1* transgenic mice display phosphorylated neurofilament aggregation and age-dependent memory impairment (Sato *et al.*, 2008), whereas *TTBK2* mutant mice manifest defects in primary cilia formation, loss of Sonic hedgehog signaling activity, and ultimately die during embryogenesis (Bouskila *et al.*, 2011; Goetz *et al.*, 2012). MAP2 and Tau are also expressed in the testes (Loveland *et al.*, 1996; Inoue *et al.*, 2014; Sigala *et al.*, 2014). However, Tau and MAP2 are detected before development of sperm flagella and with nuclear localization during meiosis (Loveland *et al.*, 1996, 1999; Inoue *et al.*, 2014). Additionally, phosphorylation of nuclear Tau at residues targeted by TTBKs is temporally observed during meiosis in the mouse male germline, suggesting that regulation of MAPs by TTBKs may contribute to early events during spermatogenesis (Inoue *et al.*, 2014). Given the potential redundancy between paralogues of TTBK and MAP2/Tau family proteins, as well as difficulties in studying *TTBK2* function in mice, uncovering the function of TTBK phosphorylation during spermatogenesis may require analyses in nonmammalian organisms.

Several studies have recently demonstrated the value of the planarian flatworm *Schmidtea mediterranea* for in vivo evaluation of genes involved in cilia formation and function (Rompolas *et al.*, 2009, 2013; Basquin *et al.*, 2015; Azimzadeh and Basquin, 2016; King and Patel-King, 2016). Planarians are free-living members of the phylum Platyhelminthes, best known for their remarkable regenerative capacity (Newmark and Sánchez Alvarado, 2002; Shibata *et al.*, 2010; Elliott and Sánchez Alvarado, 2013; Rink, 2013). Regeneration in flatworms is fueled by an adult population of pluripotent stem cells known as neoblasts. These neoblasts are the only proliferating cells of the planarian soma and undergo terminal differentiation to replace lost tissue (Saló and Baguñà, 1985, 1989; Newmark and Sánchez Alvarado, 2000; Wagner *et al.*, 2011). Not only do planarians belong to a separate phylum from organisms more commonly used in the genetic analysis of development, such as the nematode and fly (Ecdysozoa), or zebrafish, frog, and mice (Deuterostomia), but also several unique features make planarians particularly desirable in the study of cilia. For example, cellular proliferation of neoblasts occurs in the complete absence of centrosomes, and de novo development of centrioles is observed during terminal differentiation of ciliated cells (Azimzadeh *et al.*, 2012). The planarian genome has been sequenced (Robb *et al.*, 2008, 2015; Grohme *et al.*, 2018), and the distribution of expression of individual genes can be analyzed throughout the entire organism by whole-mount in situ hybridization. Gene function can be assessed systemically and by simply supplementing planarian food with double-stranded RNA targeting a specific gene (Newmark *et al.*, 2003; Reddien *et al.*, 2005; Rouhana *et al.*, 2013). Defects in the assembly or function of cilia in epidermal cells of planarians result in locomotion defects that are readily detectable and do not affect regeneration or cause immediate lethality (Reddien *et al.*, 2005; Rink *et al.*, 2009; Glazer *et al.*, 2010; Rompolas *et al.*, 2013). Last, sexual strains of *S. mediterranea* develop their entire hermaphroditic reproductive system postembryonically, offering the opportunity to analyze genetic contributions to the formation of gametes and ciliated structures of the reproductive system after embryonic development is completed (Zayas *et al.*, 2005; Wang *et al.*, 2007, 2010; Chong *et al.*, 2011; Rouhana *et al.*, 2017). In this study, we take advantage

of the unique characteristics of planarian biology to uncover potentially conserved contributions of TTBK homologues during the development of sperm and somatic ciliary structures.

RESULTS

Six TTBK homologues are encoded in the genome of *S. mediterranea* and preferentially expressed in testes

A TBLASTN search revealed six sequences with partial identity to human TTBK1 and TTBK2 (E value ≤ $2.37e^{-73}$) among contigs from a reference transcriptome assembly of the sexual strain of *S. mediterranea* (Rouhana *et al.*, 2012). All six sequences were cross-referenced to sequences in independent transcriptomes deposited in PlanMine (Brandl *et al.*, 2016), validated as individual loci in *S. mediterranea* genome sequences (Robb *et al.*, 2015; Grohme *et al.*, 2018), and named Smed-TTBK-a, -b, -c, -d, -e, and -f (Supplemental Table S1). Orthology to TTBK family proteins was confirmed using reciprocal BLASTP searches between predicted planarian translation products and human RefSeq protein sequences deposited in the National Center for Biotechnology Information (NCBI) (Supplemental Table S2). Planarian TTBKs share 61–71% protein sequence identity with human orthologues within the conserved kinase domain, whereas 85% identity is shared between human paralogues in this region (Figure 1A). In addition, conserved TTBK1 active site residues (Kiefer *et al.*, 2014), and residues that are fundamental to the structure of kinases in general (Hanks and Hunter, 1995), are present in each of the TTBK paralogues of *S. mediterranea* (Supplemental Figure 1). No conservation was detected outside of the kinase domain between planarian and human TTBK sequences. However, regions of less than 50% identity are shared between human paralogues outside of the kinase domain, and a stretch smaller than 50 amino acids with 46% identity is shared between Smed-TTBK-c and Smed-TTBK-d (Figure 1A). These analyses suggest that all six planarian TTBK homologues are active kinases that derived from an ancestral TTBK sequence, and that human paralogues are a result of a recent duplication not ancestrally present before divergence of lophotrochozoans and deuterostomes. Furthermore, the lack of sequence conservation outside of the kinase domain corroborates with observations made by Ikezu and Ikezu (2014), who proposed that current TTBK homologues arose through evolution from a shorter *TTBK* gene composed of the kinase domain. Further analysis revealed the presence of TTBK orthologues in genomes of sponges and cnidarians, indicating that this protein family is present throughout the animal kingdom (Figure 1B). Interestingly, TTBK orthologues were also found in slime molds (i.e., *Dictyostelium discoideum*, *Acytostelium subglobosum*, and *Cavenderia fasciculata*) (Figure 1B). However, TTBKs were not found in yeast (i.e., *Saccharomyces cerevisiae*, *Neurospora crassa*), the alga *Chlamydomonas reinhardtii*, or *Arabidopsis thaliana*, where the closest homologue to human TTBKs were members of the Casein Kinase I family of proteins (Figure 1B). These results suggest that *TTBK* was present in the last common ancestor shared between animals and slime molds (Mycetozoa), but may have been lost during the evolution of fungi.

We performed whole-mount in situ hybridization (WMISH) to assess the distribution of expression of *TTBK* paralogues in planarian hermaphrodites. WMISH analyses were performed on samples from a clonal sexual strain of *S. mediterranea* (Zayas *et al.*, 2005) grown to a size of ~1.3 cm, for which postembryonic development of a functional reproductive system is expected (Figure 2A). Two different riboprobes were used to analyze the expression of each *S. mediterranea TTBK* paralogue. One set corresponded to sequence complementary to the region encoding the conserved kinase domain, whereas the other set targeted transcript regions that corresponded
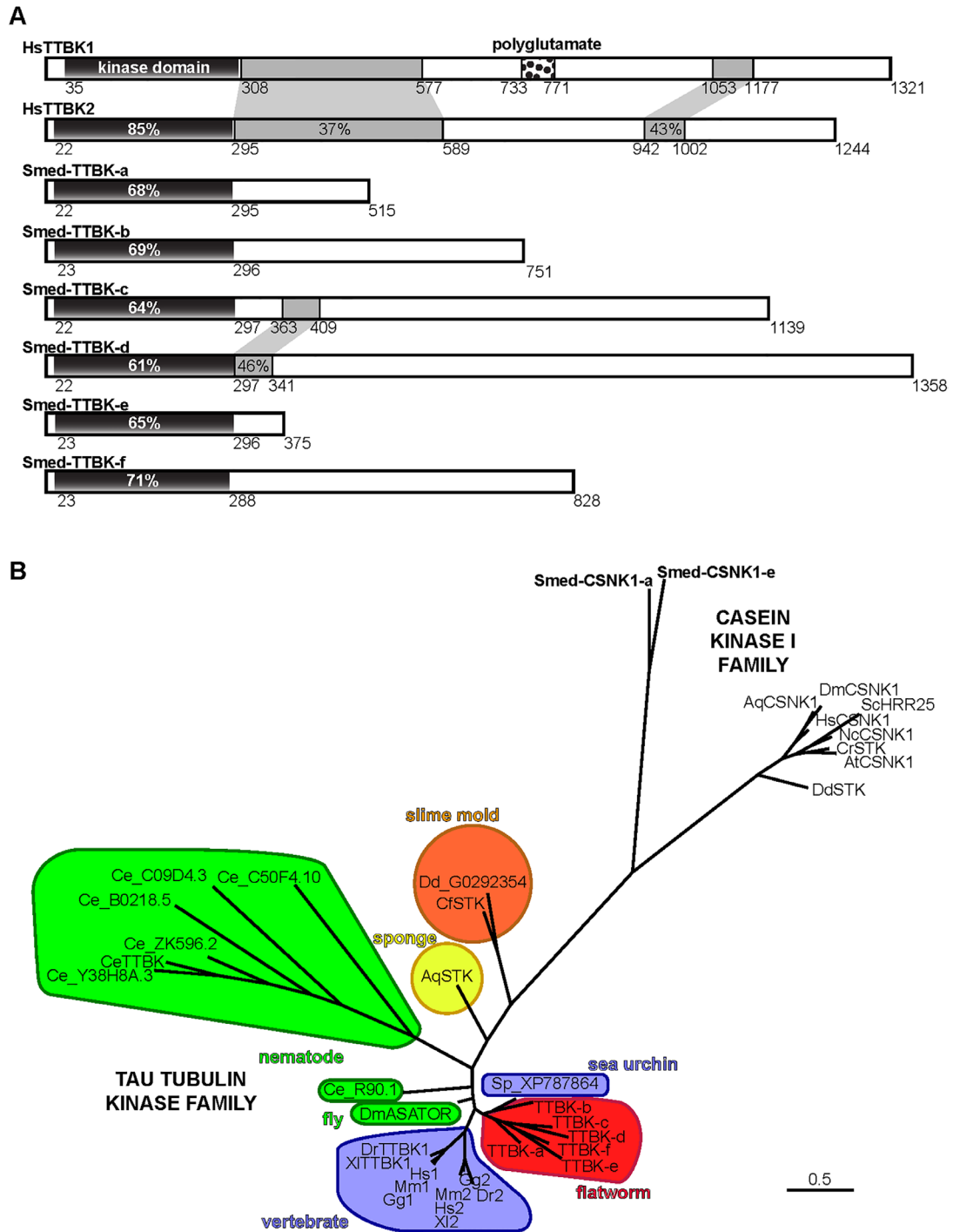
FIGURE 1: Six genes in *S. mediterranea* are homologues of TTBKs with sequence conservation limited to the kinase domain. (A) Schematic of conserved regions of predicted amino acid sequence between human and planarian TTBK homologues. Location of conserved kinase domain and percent identity relative to that of HsTTBK1 are highlighted in black. Regions of conserved sequence outside the kinase domain and corresponding percent identity are highlighted in gray. The presence of a polyglutamate domain is indicated by a dotted box. Numbering at the bottom of each diagram indicates amino acid positions. (B) Phylogenetic tree based on maximum-likelihood principle estimates depicting the recent amplification of TTBK genes in *S. mediterranea*, and the relationship between TTBK and Casein Kinase family members. Phylogenetic analysis was performed on kinase domain protein sequences using default settings in phylogeny.fr (Dereeper *et al.*, 2008). Abbreviations and shading: slime molds (orange) *D. discoideum* (Dd) and *C. fasciculata* (Cf); sponge (yellow) *Amphimedon queenslandica* (Aq); the ecdysozoans (green) *Caenorhabditis elegans* (Ce) and *Drosophila melanogaster* (Dm); the platyhelminth *S. mediterranea* (Smed; red); and the deuterostomes (blue) *Homo sapiens* (Hs), *Mus musculus* (Mm), *Gallus gallus* (Gg), *Xenopus tropicalis* (Xt), *Danio rerio* (Dr), and *Strongylocentrotus purpuratus* (Sp). TTBK homologues were not found in *S. cerevisiae* (Sc), *N. crassa* (Nc), *A. thaliana* (At), or *C. reinhardtii* (Cr), but their genomes do contain at least one Casein Kinase family I member (not shaded; top right). Scale bar = 0.5 substitutions per amino acid position.
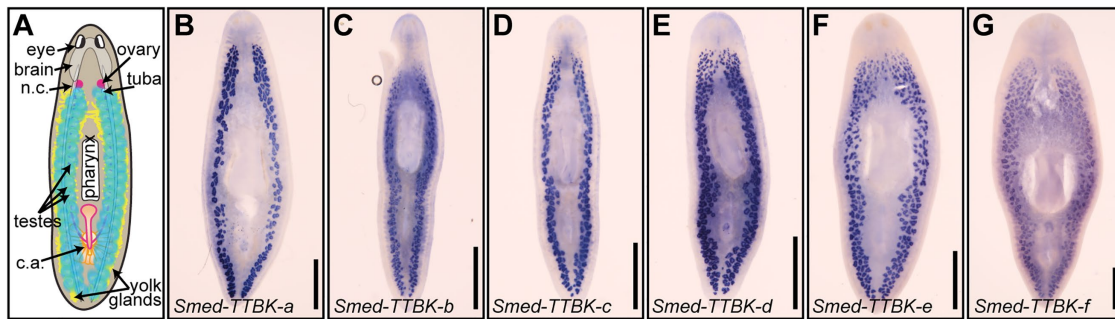
FIGURE 2: TTBK homologues are expressed in the testes of adult sexual planarians. (A) Schematic representation of the planarian body plan, including sensory organs, the pharynx, and hermaphroditic reproductive anatomy. (B–G) Distribution of expression of each of the six *S. mediterranea* TTBK paralogues is preferentially detected in the testes of sexual samples by whole-mount in situ hybridization. Abbreviations: c.a., copulatory apparatus; n.c., nerve cord. Scale bars = 1 mm.

to protein sequence not conserved between TTBK paralogues (see *Materials and Methods*). Both approaches showed identical results. Expression of each of the six *TTBK* paralogues was robustly detected in the testes, which are distributed dorsolaterally throughout most of the planarian body (Figure 2, B–G). Surprisingly, expression of *TTBK* paralogues was not conclusively detected in the brain or elsewhere in the planarian anatomy using this approach. These results demonstrate that expression of planarian *TTBK* paralogues is particularly abundant in the testes, which is a feature that is conserved with human TTBK homologues.

Expression of *Smed-TTBK-d* is essential for sperm development

To identify potential functions of *TTBK* paralogues in *S. mediterranea*, we disrupted expression of *Smed-TTBK-a, -b, -c, -d, -e,* and *-f* individually using RNA interference (RNAi). Groups of five individuals from the clonal line of *S. mediterranea* sexual strain were subjected to a diet composed of beef liver supplemented with double-stranded RNA (dsRNA) targeting specific *TTBK* paralogues. Planarians were fed twice per week for 3 wk and analyzed 7 d after the last feeding (Figure 3A). This RNAi regimen has been shown to sustain disrupted expression of target sequences systemically without having nonspecific side effects in the anatomy or physiology of planarians (Collins *et al.,* 2010; Chong *et al.,* 2013; Rouhana *et al.,* 2013, 2017; Steiner *et al.,* 2016). A negative control group was fed liver containing dsRNA corresponding to firefly *luciferase* sequence. As a positive control for RNAi penetrance, a group was fed dsRNA targeting *Smed-prohormone convertase 2 (PC2)*, which is required for proper development of the reproductive system (Collins *et al.,* 2010). At the end of the RNAi treatment, the overall appearance of planarians subjected to knockdown of *TTBK* paralogues was comparable to that of *luciferase(RNAi)* controls, with the exception of *Smed-TTBK-d* knockdown planarians (*Smed-TTBK-d(RNAi)*), which manifested abnormal motility (Supplemental Table S3). To analyze the planarian anatomy at the cellular level, RNAi
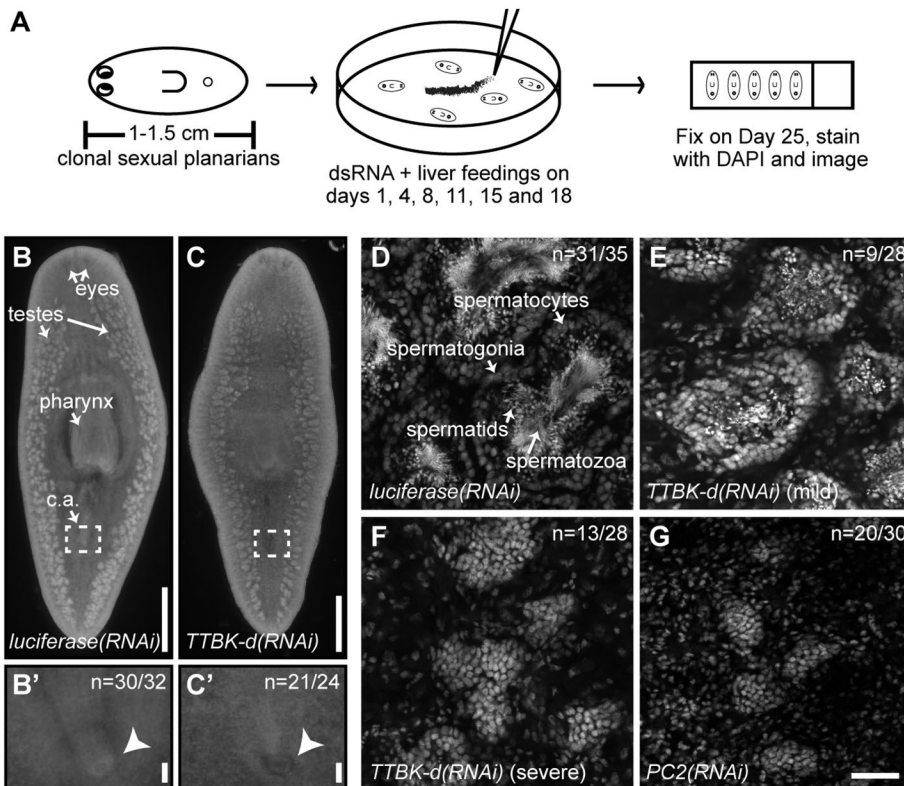

FIGURE 3: *Smed-TTBK-d* is required for spermatogenesis. (A) Schematic representation of experimental schedule in analyses of gene function by RNAi. Sexual planarians of 1–1.5 cm size were fed liver supplemented with gene-specific dsRNA six times over the course of 3 wk. After RNAi treatment, samples were stained with DAPI and imaged. (B, C) Comparable overall anatomy of *luciferase(RNAi)* (B, B') and *Smed-TTBK-d(RNAi)* (C, C') was observed in DAPI-stained samples at the end of RNAi treatments. The presence of a copulatory apparatus (c.a.) indicating sustained sexual maturity was observed in both groups (dashed rectangles in B and C and magnified view in B' and C'). (D–G) Single plane confocal images of testes region in DAPI-stained samples revealed spermatozoa accumulation in the lumen of *luciferase(RNAi)* testis lobes (D), but not in testes of *Smed-TTBK-d(RNAi)* (E, F) or *PC2(RNAi)* (G). The fraction of biological replicates that exhibited the phenotype represented in B' and C' and D–G is indicated in the top right corner of each image. Scale bars = 1 mm (B, C), 0.1 mm (B', C'), and 50 μm (D–G).

groups were fixed 1 wk after the last dsRNA feeding and stained with 4′,6-diamidino-2-phenylindole (DAPI), which labels DNA in the nucleus of cells throughout the planarian anatomy. Again, the overall anatomy, distribution of testis lobes, and the presence of a copulatory apparatus (an indicator of sexual maturity) were comparable in TTBK knockdowns and *luciferase(RNAi)* planarians (Figure 3, B, C, B′, and C′; Supplemental Table S3).

Given the preferential expression of *TTBK* paralogues in the testis, as revealed by WMISH (Figure 2, B–G), we decided to analyze the cellular anatomy of this structure in more detail by confocal microscopy. Progression of spermatogenesis in planarian testis lobes shares structurally similarities with what is observed in human seminiferous tubules (reviewed by Newmark *et al.*, 2008). Germline stem cells and spermatogonia populate and divide in the outer part of the lobe, meiosis and differentiation proceed inward, and spermatozoa with an elongated nucleus fill the innermost region (Figure 3D). Normal distribution of developing sperm with the accumulation of elongated spermatozoa was observed in testes of *luciferase(RNAi)* (Figure 3D). By contrast, testes of *Smed-TTBK-d(RNAi)* displayed irregularities in sperm development that ranged from abnormal morphology and loss of spermatozoa (mild pheno-

type; Figure 3E) to the complete loss of elongating structures (severe phenotype; Figure 3F). Small testis lobes were observed in planarians subjected to *PC2* RNAi (Figure 3G), which is known to block sexual maturation and progression of spermatogenesis from germline stem cells (Collins *et al.*, 2010). The applied RNAi protocol has been shown to decrease levels of target mRNAs by 90–95% (Counts *et al.*, 2017). However, sperm development in testes of planarians subjected to RNAi targeting expression of *Smed-TTBK-a*, *-b*, *-c*, *-e*, or *-f* appeared to be normal, and no additive effects were observed from simultaneous knockdown of *Smed-TTBK* paralogues (Supplemental Table S3). Since we cannot rule out the possibility that residual gene expression during RNAi may be sufficient to mask potential phenotypes from complete loss-of-function of TTBK paralogues, and since RNAi efficiency is known to decrease when targeting multiple planarian genes simultaneously (Higuchi *et al.*, 2008), we are unable to conclude whether other TTBK paralogues contribute to sperm development (or any other processes). However, our results demonstrate that *Smed-TTBK-d* is required for sperm development.

To determine the timing of *Smed-TTBK-d* expression during spermatogenesis more precisely, we analyzed expression of this gene by fluorescence in situ hybridization (FISH) and confocal microscopy. For reference, we included established markers of spermatogonia (germinal histone H4 (gH4); Wang *et al.*, 2007), spermatocytes (*Smed-tkn-1*; Chong *et al.*, 2011), and spermatids (*Smed-pka*; Chong *et al.*, 2011) for simultaneous analysis with *Smed-TTBK-d* (Figure 4). FISH analyses revealed that *Smed-TTBK-d* transcripts were present in spermatogonia (Figure 4, A and A″), spermatocytes (Figure 4, B and B″), and spermatids (Figure 4, C and C″). The distribution of *Smed-TTBK-d* transcript abundance more closely resembled that of *Smed-pka*, suggesting that the relative expression of *Smed-TTBK-d* peaks during the spermatid stage of spermatogenesis (Figure 4, C and C″). The peak pattern of *Smed-TTBK-d* expression corroborates with the loss of spermatid elongation observed in the testes of *Smed-TTBK-d(RNAi)* (Figure 3F). However, detection of *Smed-TTBK-d* expression in spermatogonia and spermatocytes opened the possibility that *Smed-TTBK-d* function may be required for earlier stages of spermatogenesis.

To pinpoint the earliest stage affected by disruption of *Smed-TTBK-d* expression during spermatogenesis, we analyzed the testes of *luciferase(RNAi)* and *Smed-TTBK-d(RNAi)* by whole-mount double-fluorescence in situ hybridization using genetic markers for specific stages of spermatogenesis (Figure 5). Spermatogonia (labeled by *gH4*) and spermatocytes (labeled by *tkn-1*) were observed in testes of every *luciferase(RNAi)* (Figure 5A; *n* = 7) and *Smed-TTBK-d(RNAi)* (Figure 5B; *n* = 11) sample. Analyses using the combination of spermatogonia (*gH4*) and spermatid (*pka*) markers also revealed the presence of both
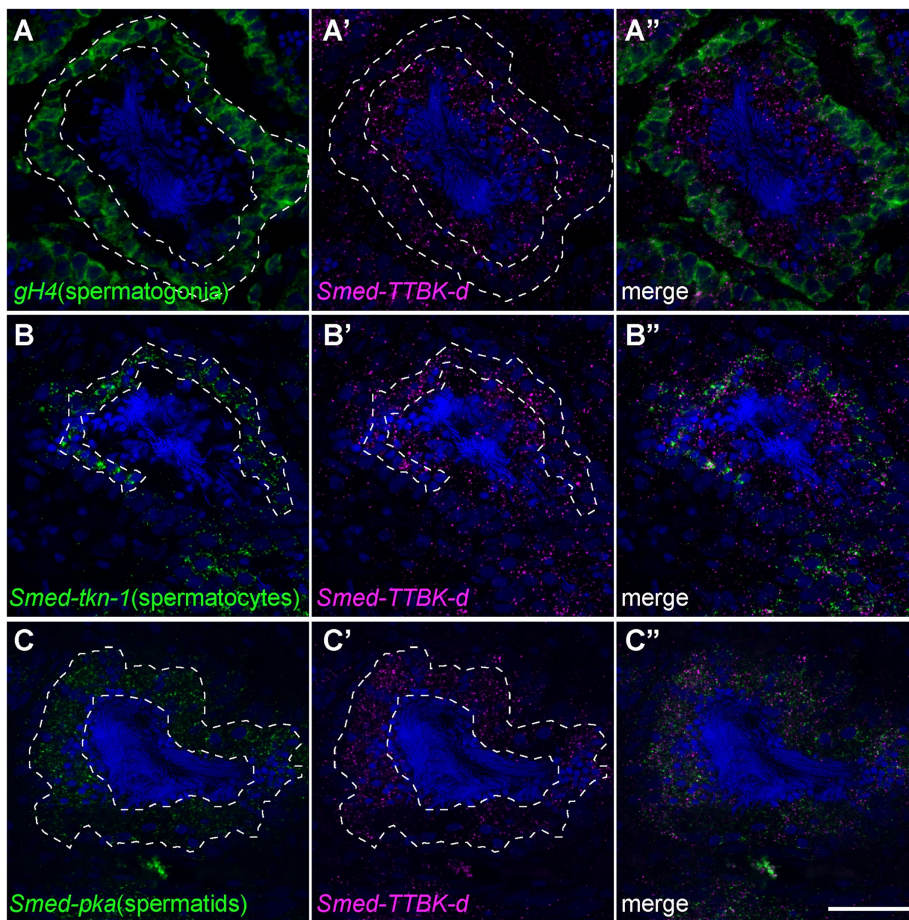
FIGURE 4: Expression of *Smed-TTBK-d* in the planarian testes is detected early during spermatogenesis and peaks in spermatids. (A–C) Single plane confocal images of double-fluorescence in situ hybridization analysis using riboprobes for markers of different stages of spermatogenesis (A–C; green) and *Smed-TTBK-d* (A′–C′; magenta). *Smed-TTBK-d* expression is detected in a subset of cells that also express the spermatogonial marker *germinal histone H4* (*gH4*; A–A″), the spermatocyte marker *Smed-tkn-1* (B–B″), and the spermatid marker *Smed-pka* (C–C″). Nuclear morphology is visualized by DAPI staining in all panels (blue). The distribution of expression for specific spermatogenesis markers in delineated (dashed lines, A, A′ to C, C′). Merged views are shown (A″–C″). Scale bar = 50 µm.

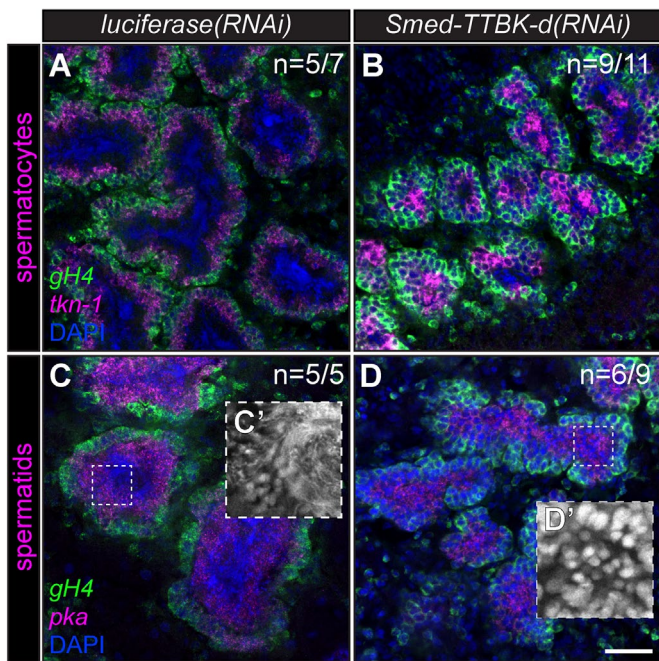**FIGURE 5:** Spermatozoa and elongating spermatids are absent in testes for *Smed-TTBK-d(RNAi)*. (A–D) Single plane confocal images of double-fluorescence in situ hybridization analysis of *luciferase(RNAi)* (A, C) and *Smed-TTBK-d(RNAi)* (B, D) planarian testes. *gH4* is used as a genetic marker of spermatogonia (A–D; green), *tkn-1* as a marker for spermatocytes (A, B; magenta), and *pka* as a marker for spermatids (C, D; magenta). Nuclear morphology and elongated spermatozoa heads are visualized by DAPI staining (blue in A–D, gray in C' and D'), and threefold magnified views are shown in C' and D'. The fraction of individuals that displayed the phenotype represented by each image is shown at the top right corner of each image. Scale bar = 50 µm.

of these cell types in testes of every *luciferase(RNAi)* (Figure 5C; n = 5) and *Smed-TTBK-d(RNAi)* (Figure 5D; n = 9) sample. As before, elongating spermatids and spermatozoa were observed by DAPI staining in the testes of most (83%) *luciferase(RNAi)* planarians (Figure 5, A, n = 5/7, and C and C'; n = 5/5), but were absent in the testes of 75% of *Smed-TTBK-d(RNAi)* (Figure 5, B; n = 9/11, and D and D'; n = 6/9). These results demonstrate that *Smed-TTBK-d* is required for spermatid elongation.

Smed-TTBK-d is required for normal planarian behavior and protonephridia function

In addition to defects in sperm development, planarians subjected to *Smed-TTBK-d* RNAi displayed behavioral and physiological irregularities not observed on knockdown of any other planarian *TTBK* paralogue or in *luciferase(RNAi)* (Figure 6, A and B; Supplemental Videos S1 and S2; Supplemental Table S3). The motility of *Smed-TTBK-d(RNAi)* planarians transitioned from gliding around their husbandry containers, as do normal and *luciferase(RNAi)* planarians (Figure 6A; Supplemental Video S1), to displaying "inch-worm" or inching-like movements (Figure 6B; Supplemental Video S2). Inching-like movements are the phenotypic manifestation of loss of functional motile cilia in epithelial cells that propel planarian gliding (Rink *et al.*, 2009; Rompolas *et al.*, 2009). In an effort to quantify differences in motility, *luciferase(RNAi)* and *Smed-TTBK-d(RNAi)* planarians were subjected to light-response behavioral analyses

based on those of Inoue *et al.* (2004, 2015). Groups of five planarians were placed in an illuminated end of a Petri dish and monitored for 3 min. Planarians subjected to *luciferase* RNAi readily moved away from the illuminated region and spent most of the time in the end of the Petri dish farthest from the light source (Figure 6, C and E), as was expected from previous observations of normal planarian behavior (Inoue *et al.*, 2004, 2015). In contrast, *Smed-TTBK-d(RNAi)* planarians remained at the most illuminated end of the Petri dish for the majority of the time period of analysis (Figure 6, D and F). These results confirmed abnormal behavior in *Smed-TTBK-d(RNAi)* and suggested that Smed-TTBK-d is required for normal gliding motility of planarians.

Partial bloating (tissue edema) was observed in regions of planarians subjected to *Smed-TTBK-d* RNAi, which suggested that protonephridia may also require proper expression of *Smed-TTBK-d*. Protonephridia are ciliated structures of the planarian anatomy that regulate water and salt content (McKanna, 1968a,b; Ishii, 1980). Bloating is a phenotype caused by the defective function of protonephridia that has been extensively characterized in asexual planarians (Rink *et al.*, 2009, 2011; Scimone *et al.*, 2011; Thi-Kim Vu *et al.*, 2015). Thus, we subjected asexual planarians to *Smed-TTBK-d* RNAi in order to verify whether expression of this gene is required for the function of protonephridia. Asexual planarians were fed twice per week for 4 wk with liver containing either *luciferase* dsRNA or *Smed-TTBK-d* dsRNA. All *luciferase(RNAi)* appeared normal a week following the last RNAi treatment (n = 17/17; Figure 7A). By contrast, the majority of *Smed-TTBK-d(RNAi)* planarians displayed either mild (n = 5/17; Figure 7B) or severe (n = 10/17; Figure 7C) bloated phenotypes. At this point, we amputated the heads and tails from *luciferase(RNAi)* and *Smed-TTBK-d(RNAi)* and waited a week to assess the regenerative capacity in these planarians. The development of photoreceptors was used as indicative of successful regeneration, which was observed in all but one *luciferase(RNAi)* trunk fragment (n = 14/15; Figure 7D). Most of the bloated planarians died after being amputated (n = 9/17), but the majority of the fragments that that did survive were able to regenerate (n = 6/8; Figure 7E), suggesting that *Smed-TTBK-d* is not directly required for stem cell-driven regeneration. Altogether, these results demonstrate that in addition to being essential for sperm development, *Smed-TTBK-d* is required in the soma for proper osmoregulation and motility.

Smed-TTBK-d is required for the structural integrity of planarian motile cilia and protonephridial units

Smed-TTBK-d expression was detected conclusively only in the testes from analyses by WMISH in sexual planarians (Figure 2E), but the behavioral phenotype of *Smed-TTBK-d(RNAi)* suggested that this gene is active in somatic cells responsible for motility and osmoregulation. To identify the somatic distribution of *Smed-TTBK-d* expression, we consulted the single-cell transcriptome analyses of asexual planarians available from Planarian SCS (https://radiant.wi.mit.edu; Wurtzel *et al.*, 2015), Planarian digiworm (https://digiworm.wi.mit.edu; Fincher *et al.*, 2018), and single-cell RNAseq data from Plass *et al.* (2018). According to the data deposited in Planarian SCS, expression of *Smed-TTBK-d* (dd_Smed_v4_12470_0_1) in asexual planarians is enriched in ciliated epithelia (epidermis II), as well as in cells of the protonephridia, and in ciliated neurons (Supplemental Figure S2). The records in Planarian digiworm also indicated enrichment of *Smed-TTBK-d* expression in neuronal and epidermal cell types (Supplemental Table S4), whereas the transcriptome studies of Plass *et al.* (2018) detected enriched expression for this gene in secretory cells (secretory 2 category), cells of the
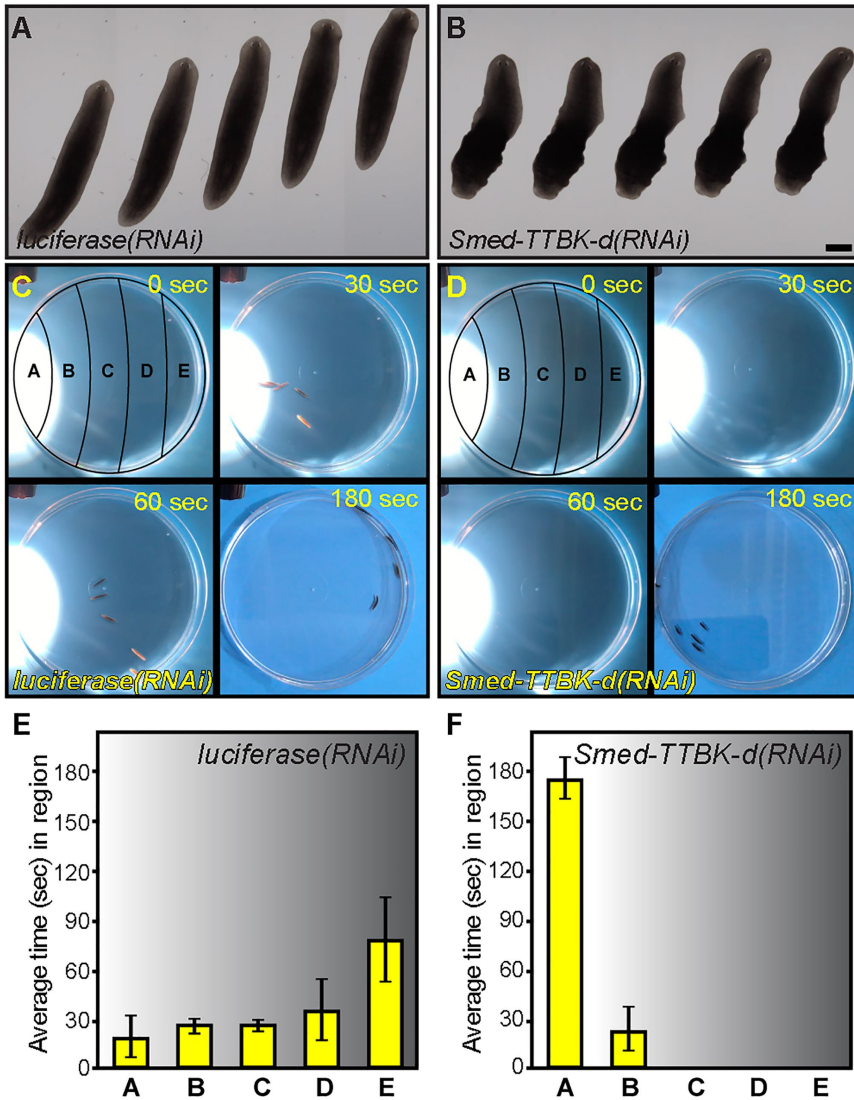
FIGURE 6: *Smed-TTBK-d* is required for normal locomotion. (A, B) Series of live images (an image per second) showing that the extended posture and gliding motility of *luciferase(RNAi)* controls (A) are lost in *Smed-TTBK-d(RNAi)* (B) sexual planarians. (C, D) Video still captures indicating the position of different planarians at 0-, 30-, 60- and 180-s time points during a light-response test, illustrating the migration away from the light observed in *luciferase(RNAi)* (C), but not in *Smed-TTBK-d(RNAi)* (D). Planarians were placed in the illuminated region (labeled "A") at the 0-s time point. (E, F) Quantitation of average length of time that *luciferase(RNAi)* (E) and *Smed-TTBK-d(RNAi)* (F) spent in each region of the arena in assays such as the ones shown in C and D ($n \geq 10$ biological replicates). Error bars indicate SD of the mean. Scale bar = 1 mm (A, B).

region where nonspecific background is often observed during planarian WMISH analyses (Figure 8B). The expression of *Smed-TTBK-d* in epithelial cells was validated in sexual planarians by FISH (Figure 8, C and D). These results confirm the expression of *Smed-TTBK-d* in cells of the planarian epidermis and suggest that the behavioral defects observed in *Smed-TTBK-d(RNAi)* could be due at least in part to abnormal development or function of epidermal motile cilia.

To determine whether structural abnormalities exist in multiciliated epidermal cells of *Smed-TTBK-d(RNAi)*, we visualized the distribution of cilia using anti–acetylated-tubulin antibodies (anti-AcTub) as per Sánchez Alvarado and Newmark (1999), Rink *et al.* (2011), and Ross *et al.* (2018). We readily detected ciliary projections in the dorsal, ventral, and peripheral epithelium of *luciferase(RNAi)* planarians (Figure 8, E, G, and I). Conversely, *Smed-TTBK-d(RNAi)* planarians appeared to have lost most of the cilia in the dorsal, ventral, and peripheral epithelium (Figure 8, F, H, and J). Detection of cilia in the auricles and the dorsal ciliated stripe, which are anatomical regions hypothesized to contain a high density of ciliated sensory neurons, was reduced in *Smed-TTBK-d(RNAi)* planarians as compared with *luciferase(RNAi)* controls (Figure 8, E and F). Finally, irregularities in the morphology of structures decorated by anti-AcTub in protonephridial units, which are largely composed of motile cilia, were also observed in *Smed-TTBK-d(RNAi)* (Figure 8, K and L). These results demonstrate that *Smed-TTBK-d* RNAi is required for the proper formation of ciliated structures involved in planarian motility, behavior, and fluid homeostasis.

To better characterize the defects in cilia formation observed on *Smed-TTBK-d(RNAi)*, we analyzed multiciliated ventral epithelial cells by anti–α-tubulin immunofluorescence and high-magnification confocal microscopy (as per Rompolas *et al.*, 2010, 2013; and Vij *et al.*, 2012). Control *luciferase(RNAi)* planarians possessed filamentous cilia of homogeneous dimensions distributed throughout the regions of peripheral ventral epidermis (Figure 9A). By comparison, the structures illuminated by anti–α-tubulin immunofluorescence in analogous cells of *Smed-TTBK-d(RNAi)* planarians were less densely distributed and varied in thickness and architecture from normal epidermal cilia described in the literature (Figure 9B; Rompolas *et al.*, 2009, 2010; Almuedo-Castillo *et al.*, 2012; Rompolas *et al.*, 2013). Three-dimensional analysis by digital stitching deconstruction of confocal images taken at different planes along the z-axis (i.e., z-stacks) revealed a gap of ~10 µm between the nuclei of these cells and the region of cilia illuminated by anti–α-tubulin in *luciferase(RNAi)* planarians (Figure 9A'). However, the distance between the nucleus and the ciliary structures illuminated

pharynx and the epidermis, as well as GABAergic and cholinergic neurons. To circumvent potential issues caused by strong signal detection in the testes during validation of *Smed-TTBK-d* expression in other tissues, we performed WMISH in asexual planarians. We used a riboprobe against *Smed-pka* as a control for nonspecific background in asexual planarians. *Smed-pka* is a well-established marker of spermatids in sexual planarians (Chong *et al.*, 2011), and no matching records are found in transcriptomes of asexual *S. mediterranea* deposited in PlanMine (dd_v4; Liu *et al.*, 2013; others). Expression of *Smed-TTBK-d* was detected in the head, the pharynx, and the periphery of the planarian body after overnight development of WMISH signal (Figure 8A). By contrast, signal detection from *Smed-pka* expression emerged only from the gut, which is a
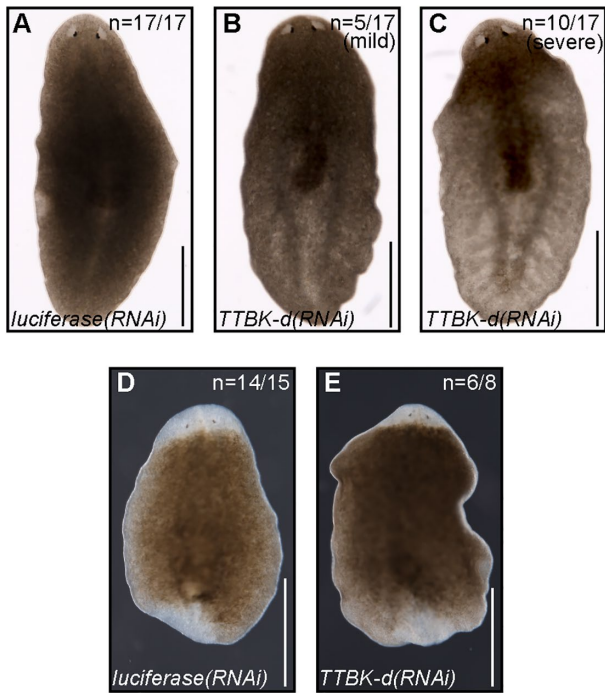
FIGURE 7: Asexual planarians subjected to *Smed-TTBK-d* RNAi develop a bloating phenotype representative of defects in protonephridia function. (A–C) Asexual planarians imaged by bright-field microscopy exhibit normal anatomical features after a 3-wk treatment of *luciferase* dsRNA (A), whereas planarians subjected to dsRNA targeting *Smed-TTBK-d* developed mild (B) and severe (C) bloating phenotypes. (D, E) Trunk fragments with regenerated heads and tails imaged by dark-field microscopy 7 d after amputation. Representative images of *luciferase(RNAi)* (D) and *Smed-TTBK-d(RNAi)* (E) trunk fragments able to regenerate heads and tails (unpigmented tissue) 7 d postamputation. The fraction of planarians represented by the imaged phenotype is indicated the top right corner of each frame in A–E. Planarians that did not survive 48 h postamputation and were excluded from the denominator in D and E. Scale bar = 1 mm.

by anti–α-tubulin in cells of the ventral epidermis was not present in *Smed-TTBK-d(RNAi)* (Figure 9B'). To get a better sense of the position of abnormal cilia structures found in ventral epidermal cells of *Smed-TTBK-d(RNAi)*, we costained samples with a lectin dye that labels epidermal cell junctions in *S. mediterranea* (concanavalin A [ConA]; Zayas *et al.*, 2010). ConA staining revealed that the region of cilia stained by anti–α-tubulin protrudes distal to the edge of the cytoplasmic region in *luciferase(RNAi)* samples (Figure 9C). On the other hand, the structures illuminated by anti–α-tubulin in *Smed-TTBK-d(RNAi)* planarians remain within the cytoplasm of the ventral epidermis and do not extend past the epidermal cell surface (Figure 9D). These results suggest that *Smed-TTBK-d* is required for maintaining the structure, density, and position of cilia in multiciliated epithelial cells of *S. mediterranea*.

Multiple indirect analyses indicated that *Smed-TTBK-d* is essential to the structure (i.e., immunofluorescence using anti-AcTub and anti–α-tubulin) and function (i.e., phenotypic manifestation inchworm movements, bloating) of motile cilia in planarian somatic tissues. To assess the integrity of motile cilia directly, we first mounted live asexual planarians on slides as per Rompolas *et al.* (2010) and performed live imaging recordings by phase contrast microscopy (Supplemental Videos S3 and S4). As expected, motile cilia were readily observed in the periphery of *luciferase(RNAi)* planarians and in particular around the head region (Figure 9E; Supplemental Video S3). Conversely, only a few cilia, which displayed slight motility, were observed in the periphery of *Smed-TTBK-d(RNAi)* (Figure 9F; Supplemental Video S4). Next, we analyzed ciliary structures in planarian epidermis by transmission electron microscopy (TEM) (Figure 9, G and H). We observed multiple axonemal projections of typical 9 + 2 microtubule arrangement, as well as basal bodies docked to the plasma membrane, in epidermal cells of *luciferase(RNAi)* micrographs (Figure 9G). By contrast, basal bodies and axonemal projections were rarely found in the micrographs of *Smed-TTBK-d(RNAi)* (Figure 9H). Instead, we observed multiple abnormal projections (Figure 9H, empty arrowheads) and presumptive rootlets that were not connected to basal bodies or cilia (Figure 9H', white arrows). These results demonstrate that *Smed-TTBK-d* expression is required for the proper assembly of motile cilia and suggest that Smed-TTBK-d may function in both basal body assembly and axoneme formation.

Expression of MAP2/TAU homologues in testes of *S. mediterranea*

Our data suggest that *Smed-TTBK-d* contributes to the initiation and assembly of motile cilia/flagella through conserved mechanisms reported for mammalian TTBK2 during the development of primary cilia (Goetz *et al.*, 2012; Bowie *et al.*, 2018). Homologues of centriolar proteins that interact with mammalian TTBKs during the regulation of primary cilia formation (i.e., CP110 and Cep164; Goetz *et al.*, 2012; Cajanek and Nigg, 2014; Oda *et al.*, 2014) have been shown to be required for normal motility in *S. mediterranea* (Azimzadeh *et al.*, 2012). To gain further insight into the potential roles of other well-known TTBK targets during spermatogenesis and motile cilia formation, we looked for *S. mediterranea* homologues of the MAP2/Tau microtubule-associated protein family. Neuronal members of the MAP2/Tau protein family are known TTBK substrates in mammals (Takahashi *et al.*, 1995; Sato *et al.*, 2006) and show dynamic phosphorylation at target residues during spermatogenesis (Inoue *et al.*, 2014). Three MAP2/Tau homologues were identified in reference transcriptomes of sexual and asexual *S. mediterranea* (Supplemental Table S5). These three genes, hereafter referred to as *S. mediterranea MAP2/Tau-like-1* (*Smed-MAPT-L1*), *Smed-MAPT-L2*, and *Smed-MAPT-L3*, encode for proteins that do not group with specific vertebrate MAP2/Tau family proteins (i.e., MAP2, MAP4, or Tau) in phylogenetic analyses (Figure 10A), suggesting that vertebrate and planarian MAPs emerged from independent gene duplication events. Tubulin-binding domain repeats can be identified in each of the proteins encoded by *Smed-MAPT-L* genes (three in *Smed-MAPT-L1*, four in *Smed-MAPT-L2*, and three in *Smed-MAPT-L3*) (Figure 10B; Supplemental Figure S3). The core tubulin-binding motif KXGS (Sundermann *et al.*, 2016) is present in a subset of repeats in each planarian MAPT-L paralogue (Supplemental Figure S3). Additionally, the consensus phosphorylation site for CK1 kinase isoforms (S/T*-X-X-S/T, where the asterisk marks the target residue; Flotow and Roach, 1989; Flotow *et al.*, 1990; Nakielny *et al.*, 1991), as well as preferred substrate sites for mammalian TTBK2 (S/T*-X-pY, where a primed phosphotyrosine is found at the +2 position; Bouskila *et al.*, 2011), are both present within the tubulin-binding repeats of Smed-MAPT-L3 and outside of the tubulin-binding repeats of Smed-MAPT-L1 (Figure 10B; Supplemental Figure S3). These primary sequence analyses indicate that the regulatory circuitry among TTBKs, MAP2/Tau, and tubulin may participate in directing microtubule dynamics in *S. mediterranea*.
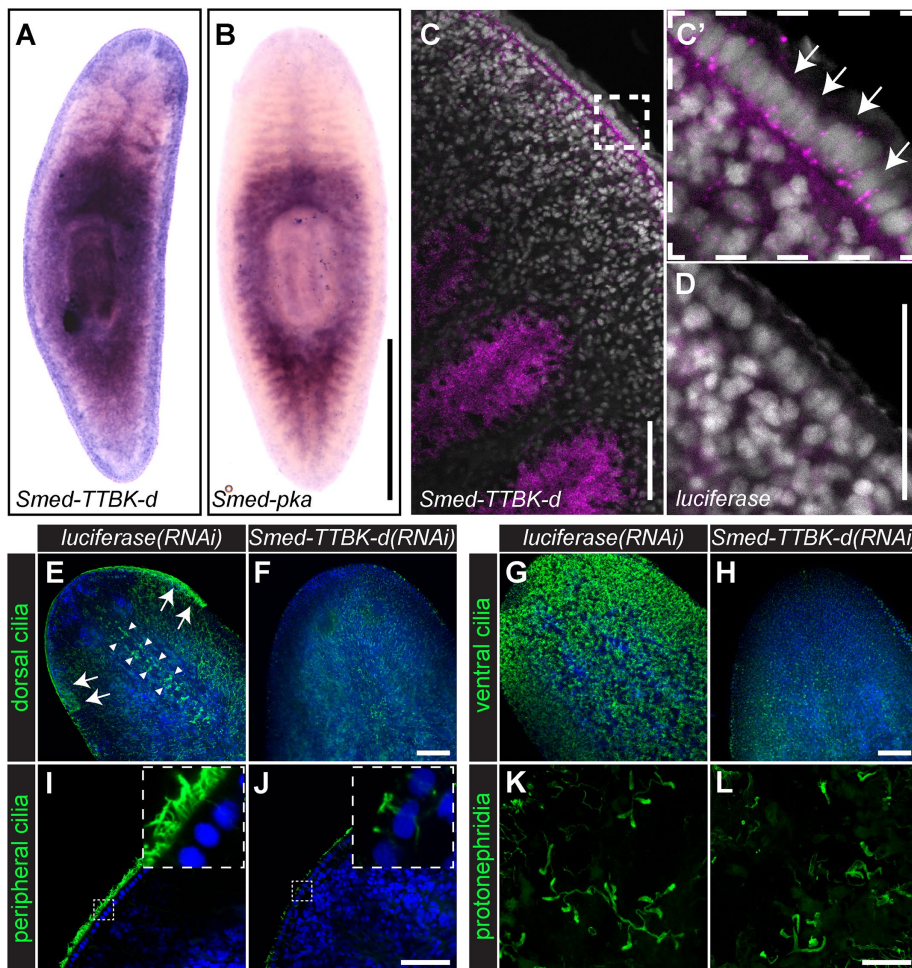
FIGURE 8: *Smed-TTBK-d* is required for normal development of ciliated epithelia and protonephridia. (A, B) Colorimetric in situ hybridization in asexual *S. mediterranea* reveals *Smed-TTBK-d* expression in the periphery of the planarian body, where ciliated epithelia reside (A). Expression of *Smed-pka*, a spermatid marker used as negative control, is not detected in the planarian periphery (B). (C, D) Confocal plane showing detection of *Smed-TTBK-d* mRNA (magenta; C and C') in peripheral epithelial cells (arrows in C') of sexual planarians analyzed by fluorescence in situ hybridization. Magnified view of area marked by a dashed square is shown C'. Specificity of *Smed-TTBK-d* transcript detection in epithelial cells is verified by parallel analysis using *luciferase* riboprobes as a negative control (magenta; D). (E–L) Maximum projections of confocal z-sections reveal ciliary structures in *luciferase(RNAi)* (E, G, I, and K) that are lost in *Smed-TTBK-d(RNAi)* (F, H, J, and L). Cilia decorated with acetylated-tubulin antibodies (green) in the dorsal (E, F), ventral (G, H), and peripheral epithelium (I, J) of asexual planarians are more prevalent in *luciferase(RNAi)* (E, G, and I) than in *Smed-TTBK-d(RNAi)* (F, H, and J). Fivefold magnified view of area marked by a dashed square is shown in insets for I and J. Cilia in areas of high sensory neuron density along the dorsal midline (arrowhead) and auricles (arrows) are indicated in (E). Acetylated-tubulin staining also reveals defects in the anatomy of protonephridial units of *Smed-TTBK-d(RNAi)* (L) as compared with those in *luciferase(RNAi)* controls (K). Cell nuclei labeled by DAPI are shown in white (C, D) and blue (E–J). Scale bars = 1 mm (A, B); 100 μm (C, E-H); and 50 μm (D, I–L).

To determine whether MAP2/Tau homologues are coexpressed with *Smed-TTBK-d*, we consulted the above-mentioned sexual planarian transcriptome (Rouhana et al., 2017) and asexual planarian single-cell RNAseq analyses (Wurtzel et al., 2015; Fincher et al., 2018; Plass et al., 2018). Transcriptomic data for *Smed-MAPT-L1* (Contigs 39776, 52868, and 33308 in the sexual strain reference transcriptome from Rouhana et al., 2012) suggested that expression of this MAP2/Tau homologue is not enriched in reproductive tissues (Supplemental Table S5). No matching contigs were found for *Smed-*

MAPT-L2 and *-L3* in the same sexual planarian reference transcriptome or analysis mentioned above (Supplemental Table S5). However, transcriptome comparisons between *S. mediterranea* sexual and asexual strains performed by Davies et al. (2017) indicate that expression of these paralogues is enriched in sexual planarians (3.4-fold enrichment for *Smed-MAPT-L2*, dd_Smed_v4_32444_0_2; and 3.2-fold enrichment for *Smed-MAPT-L3*, dd_Smed_v4_33588_0_2). Single-cell RNAseq data from asexual planarians from Wurtzel et al. (2015) and Fincher et al. (2018) indicate that *Smed-MAPT-L1* is expressed at highest levels in neural and muscle cells (Supplemental Figure S4; Supplemental Table S4), as well as in some *cathepsin+* cells (Supplemental Table S4). Records for *Smed-MAPT-L2* and *-L3* expression in these single-cell RNAseq analyses were also either unavailable (Planarian SCS) or not enriched at significant levels in any cell type (Planarian digiworm; Supplemental Table S4). The single-cell expression analysis from Plass et al. (2018) indicates enriched expression for *Smed-MAPT-L1* in several neuronal precursors and some specified neuronal cell types (e.g., GABAergic neurons that also express *Smed-TTBK-d*), as well as in a subtype of parenchymal cells (Supplemental Figure S5). This same study detected modest, but enriched, expression of *Smed-MAPT-L2* in precursors of both muscle and epidermal cells (but not in terminally differentiated cells), as well as enriched expression of *Smed-MAPT-L3* in a specific subset of neurons (npp-18+ neurons) (Supplemental Figure S5). Altogether, these analyses suggest that overlapping expression of *Smed-TTBK-d* and *Smed-MAPT-L* genes is likely to occur in a subset of neurons, temporally during epidermal differentiation, and potentially in reproductive structures.

To directly test whether MAP2/TAU homologues are expressed in the planarian testes, we performed WMISH analyses of *Smed-MAPT-L1*, *-L2*, and *-L3* expression in sexual planarians (Figure 10, C–E). Expression of *Smed-MAPT-L1* was detected broadly in the head and throughout most of the body of sexual planarians (Figure 10C). No particular tissues were distinguishable from the distribution of *Smed-MAPT-L1* detection by WMISH, but this may be reflective of a combination of expression in neurons, muscle, *piwi+*, parenchymal, and/or *cathepsin+* cells, as observed in single-cell RNAseq analyses (Supplemental Figures S4 and S5; Supplemental Table S4). On the other hand, expression of *Smed-MAPT-L2* and *-L3* was clearly enriched in the testes of sexual planarians (Figure 10, D and E). In addition, *Smed-MAPT-L3* expression was detected in foci distributed from the posterior region of the head to the tail of the planarian body, but excluded in the pharynx and copulatory apparatus (Figure 10, E and
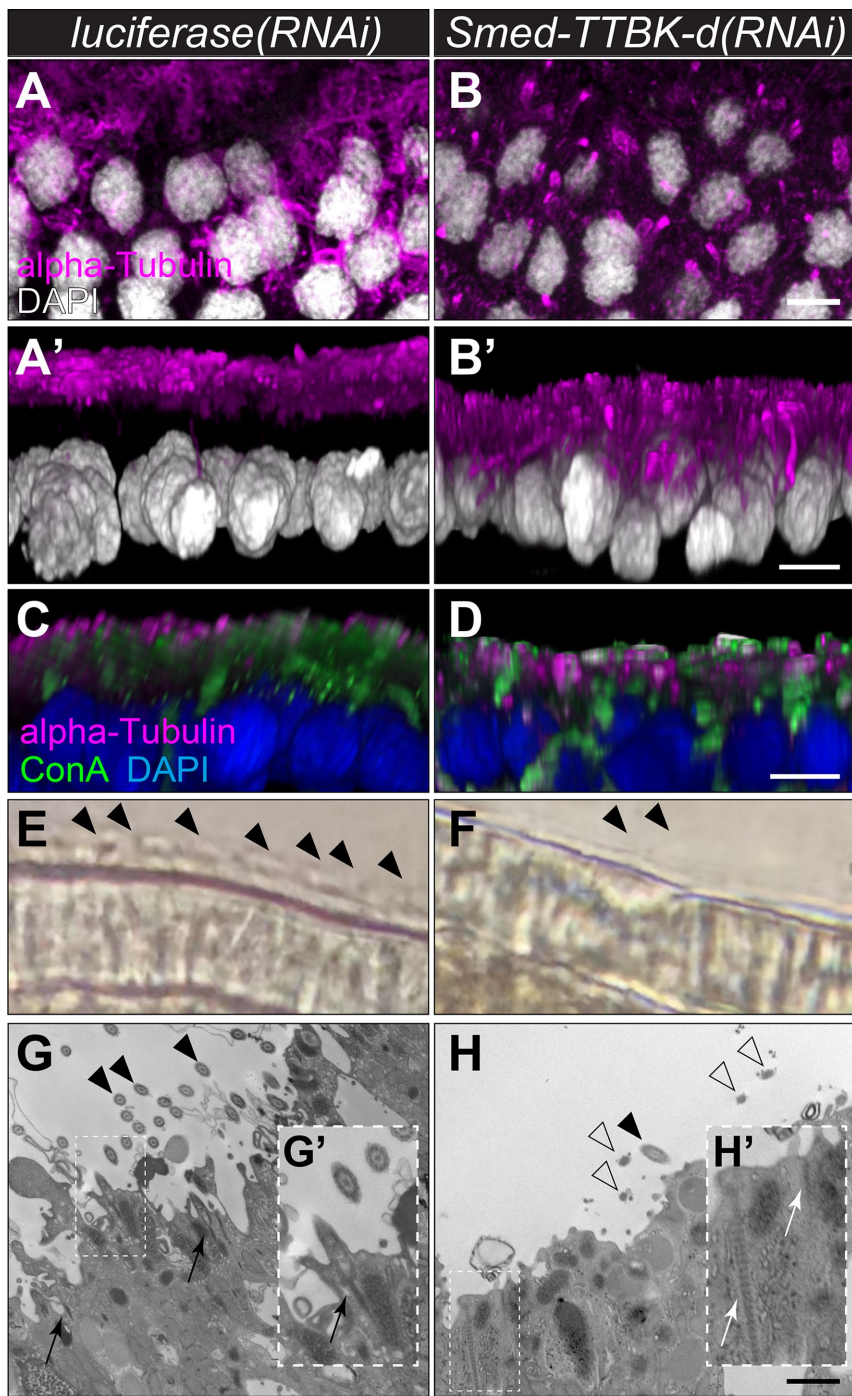
E'). These results demonstrate that expression of MAP2/Tau homologues in the testes is a shared feature between planarians and mammals, which suggests the presence of conserved tissue-specific functions for these microtubule regulators outside of the brain. We considered the possibility that *Smed-TTBK-d* may work with *Smed-MAPT-L2* and/or *Smed-MAPT-L3* in the male germline of planarians. However, functional assessment of planarian MAP2/Tau homologues by RNAi failed to support the hypothesis that *Smed-MAPT-L1*, *-L2*, or *-L3* is required for the development of spermatozoa, as testes morphology of individual, double, and triple knockdowns was comparable to that of *luciferase(RNAi)* (Supplemental Figure S6).

DISCUSSION

This study documents the characterization of six TTBK protein subfamily members expressed in the testes of *S. mediterranea*. Analysis of TTBK orthologues suggests that genetic expansion of *TTBK* genes is not ancestral among metazoans (Figure 1B). Pairwise comparison of planarian and human TTBKs found no evidence for selective pressure outside of the kinase domain (Figure 1A). These observations corroborate with the hypothesis proposed by Ikezu and Ikezu (2014) regarding the emergence of this subfamily from a protein composed mainly of the kinase domain. Taking into consideration that 1) defects in motile cilia formation are observed on knockdown of *Smed-TTBK-d*, 2) TTBK2 function is required during primary cilia formation in mice (Goetz *et al.*, 2012; Bowie *et al.*, 2018), and 3) primary sequence conservation between planarian and mammalian TTBKs is observed only in the kinase domain, we postulate that the kinase domain is sufficient for the function of TTBKs during cilia formation (be it primary or motile). Given the functional similarities and high degree of sequence conservation between the kinase domain of Smed-TTBK-d and human homologues (61% for TTBK1; 63% for TTBK2), it seems promising to consider the use of planarians in screens for potential therapeutic agents that can modulate the activity of TTBKs.

Interestingly, *Smed-TTBK-d* was the only gene of six TTBK paralogues that resulted in detectable phenotypes on RNAi. Differences in behavior, motility, osmoregulation, and sperm development were observed in *Smed-TTBK-d(RNAi)*, but not on knockdown of *Smed-TTBK-a*, *-b*, *-c*, *-e*, or *-f* (Figures 3, 6, and 7; Supplemental Table S3). The possibility of functional redundancy was tested by

FIGURE 9: *Smed-TTBK-d* is required for assembly and normal architecture of ciliated structures. (A–D) Maximum projection of confocal z-sections shows that the architecture of epithelial ciliary structures decorated by alpha-tubulin antibody staining (magenta) in *luciferase(RNAi)* (A) is distorted in *Smed-TTBK-d(RNAi)* (B). Transverse views of z-stack confocal projections of samples (A, B) reveal differences in distance between the nucleus (white) and presumptive ciliary structures (magenta) in epithelial cells of *luciferase(RNAi)* (A') and *Smed-TTBK-d(RNAi)* (B'). (C, D) Concanavalin A staining (green) reveals that ciliary structures visualized using alpha-tubulin antibodies protrude from the cell membrane in control *luciferase(RNAi)* cells (C), but are proximally misplaced in *Smed-TTBK-d(RNAi)* (D). Cell nuclei are labeled by DAPI staining (grayscale in A and B and A' and B'; blue in C and D). (E, F) Video still captures of epithelial cilia (arrows) as seen in during live imaging analysis of *luciferase(RNAi)* (E) and *Smed-TTBK-d(RNAi)* (F) by phase contrast microscopy (shown in Supplemental Videos S3 and S4). (G, H) Transmission electron micrographs showing basal body of cilia (black arrows) anchored to the epithelial cell membrane and extended axonemes (black arrowheads) in a representative section of *luciferase(RNAi)* (G),

whereas *Smed-TTBK-d* epithelial cells (H) are surrounded by aberrant axonemes (empty arrowheads) and contain presumptive uncommitted rootlets (white arrows) in their cytoplasm. Insets showing 200% magnified view of regions marked by dashed lines (G' and H'). Scale bars = 10 µm (A–D) and 500 nm (G and H).
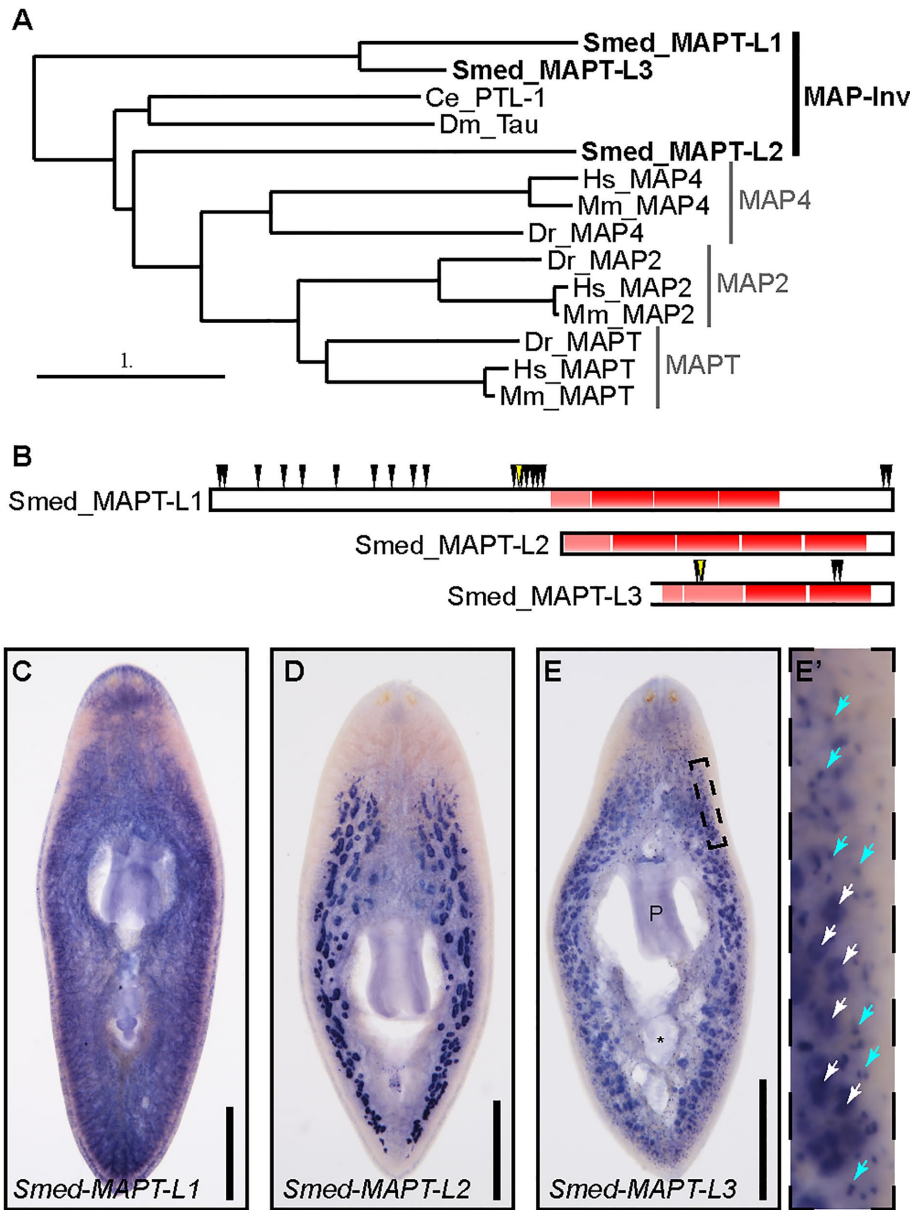
FIGURE 10: Two MAP2/Tau homologues are preferentially expressed in planarian testes. (A) Phylogenetic tree based on maximum-likelihood principle illustrates the relationship between primary sequences of characterized invertebrate MAP2/Tau (MAP-Inv) proteins in *C. elegans* (Ce), *D. melanogaster* (Dm), and *S. mediterranea* (Smed), as well as vertebrate MAP4, MAP2, and MAP-Tau orthologues in *H. sapiens* (Hs), *M. musculus* (Mm), and *D. rerio* (Dr). Scale bar = 1 substitution per amino acid position. (B) Schematic representation of MAPT-L proteins in *S. mediterranea* indicating complete (red boxes) or partial/divergent (pink boxes) tubulin-binding domain repeats identified in during BLAST analyses. Location of predicted phosphorylation sites for Casein Kinase 1 isoforms (black arrowheads) and TTBK (open arrowheads) is also indicated (see Supplemental Figure S3 for further details). (C–E) Broad distribution of expression of *Smed-MAPT-L1* is detected in whole-mount in situ hybridization samples of sexual *S. mediterranea* (C), whereas detection of *Smed-MAPT-L2* (D) and *Smed-MAPT-L3* (E) expression is enriched in the testes. Magnified view (E′) of boxed region in E reveals expression of *Smed-MAPT-L3* in testis lobes (white arrows) as well as foci of unknown cellular identity (blue arrows) located peripheral to the distribution of testes. Position of the pharynx (P) is indicated in E. Scale bars = 1 mm.

performing simultaneous knockdown with some combinations of *Smed-TTBK* paralogues, but these did not yield evidence to support cooperative or redundant functions among the different planarian TTBKs (Supplemental Table S3). Although not all possible combina-

tions were tested, aberrant phenotypes were only observed in RNAi treatments that included dsRNA targeting *Smed-TTBK-d*. Furthermore, the spermatogenesis and motility phenotypes observed on simultaneous knockdown of all six *Smed-TTBK* paralogues were indistinguishable from knockdown of *Smed-TTBK-d* alone. These observations suggest that there is something unique about *Smed-TTBK-d* expression or the specificity of interactions that makes it particularly important for the development of sperm and epidermal motile cilia. Single-cell transcriptome analyses suggest that specificity of cell-type expression may contribute to *Smed-TTBK-d* being required for osmoregulation and locomotion. The analyses from Wurtzel *et al.* (2015) suggest that *Smed-TTBK-d* is the only TTBK paralogue preferentially expressed in protonephridia, whereas *Smed-TTBK-d* and *Smed-TTBK-c* are preferentially expressed in ciliated epithelia (Supplemental Figure S2). On the other hand, the data from Fincher *et al.*, (2018) indicate that *Smed-TTBK-d* is preferentially expressed in epidermal cells and the pharynx, whereas *Smed-TTBK-c* is expressed in the protonephridia (Supplemental Table S4). Enriched expression of all six paralogues was detected in neural clusters by single-cell analysis approaches (Supplemental Figure S2; Supplemental Table S4). Conversely, the question of possible redundancy among TTBK paralogues during spermatogenesis is less clear, since all six of these genes are preferentially expressed in the testes (Figure 2), but our functional analyses only supported the requirement of *Smed-TTBK-d* during sperm development. One possibility could be that *Smed-TTBK-d* expression during spermatogenesis is much higher than that of its paralogues, but average expression values from RNA-seq analyses show that *Smed-TTBK-d* transcript abundance is actually the lowest from the six paralogues in sexual planarians (Supplemental Table S5). Given that *Smed-TTBK-d* does not seem to be expressed differently from its paralogues during spermatogenesis (at least at the transcriptional level), we hypothesize that the primary structure of Smed-TTBK-d bestows it with unique biochemical characteristics that are particularly important during sperm development. Unfortunately, we are unable to test this hypothesis due to current technical limitations with transgenesis for the study of gene function in planarians.

Smed-TTBK-d RNAi resulted in the loss of elongating spermatids and spermatozoa in the testes of 58% of our *Smed-TTBK-d(RNAi)* samples (n = 28/48; Figures 3E and 5, B and D). Detailed analysis using stage-specific markers revealed that the disruption of

spermatogenesis observed on *Smed-TTBK-d* RNAi occurs after meiosis (Figure 5D). We hypothesize that spermatid elongation in *Smed-TTBK-d(RNAi)* testes is halted due to a failure in flagellar formation under reduced *Smed-TTBK-d* activity. Although our current readout of spermatid elongation is based on the morphological transition of round nuclei into the thinly stretched structure seen in spermatozoa (Figure 3D), defects in sperm tail formation have been shown to affect sperm head shape (Lehti *et al.*, 2013). We further hypothesize that Smed-TTBK-d contributes to flagella formation through shared mechanisms active during the initial stages of cilia assembly in planarian epithelial cells (Figure 9, B, D, F, and H) and primary cilia in mammals (Goetz *et al.*, 2012; Bowie *et al.*, 2018).

Asator is an essential TTBK homologue in *Drosophila* that localizes to the mitotic spindle and interacts with spindle matrix proteins, presumably to regulate microtubule spindle dynamics (Qi *et al.*, 2009). Both MAP2 and Tau can be phosphorylated by TTBKs (Takahashi *et al.*, 1995; Tomizawa *et al.*, 2001; Sato *et al.*, 2006) and are expressed in germ cells of mammalian testes (Ashman *et al.*, 1992; Gu *et al.*, 1996; Loveland *et al.*, 1996; Inoue *et al.*, 2014). In rat testes, MAP2 is found in the nucleus of spermatocytes and round spermatids (Loveland *et al.*, 1996), and changes in Tau nucleocytoplasmic localization correlates with dynamic phosphorylation during spermatogenesis in mice (Inoue *et al.*, 2014). Phosphorylation of Tau during meiosis includes TTBK substrate residues associated with hyperphosphorylation in Alzheimer's disease (Tomizawa *et al.*, 2001; Inoue *et al.*, 2014). Thus, we considered the possibility that *Smed-TTBK-d* may regulate microtubule spindle dynamics during meiosis, and that planarian homologues of MAP4 (which contributes to spindle stability; Samora *et al.*, 2011) may be involved in this process. Two lines of evidence contradict this hypothesis. First, spermatid development is observed using stage-specific spermatogenesis markers in *Smed-TTBK-d(RNAi)* planarians (Figure 5D), indicating that completion of meiosis is not inhibited by the loss of *Smed-TTBK-d* function. Second, although testicular expression of MAP2/4/Tau homologues is conserved in planarians (Figure 10, D and E), knockdown of *Smed-MAPT-L2* and *Smed-MAPT-L3*, individually or in combination, did not reveal any defects in spermatogenesis (Supplemental Figure S6). An alternative mechanism that has not been ruled out to explain the requirement of *Smed-TTBK-d* during spermatogenesis is the potential involvement of TTBK substrates that are not MAPs. These could include homologues of the transactive response DNA-binding protein 43 kD (TDP-43; Liachko *et al.*, 2014; Taylor *et al.*, 2018), which is known to function in sperm development in mice (Lalmansingh *et al.*, 2011). Nevertheless, our preferred hypothesis is that *Smed-TTBK-d* is required for spermatid elongation through its role in flagellar assembly.

MATERIALS AND METHODS
Planarian cultures
A hermaphroditic clonal line of *S. mediterranea* (Zayas *et al.*, 2005) was used for all experiments, except where the use of individuals from the asexual strain (Sánchez Alvarado *et al.*, 2002) was specified. Laboratory populations of sexual *S. mediterranea* were expanded by amputation and maintained at 18°C in 0.75× Montjuïc salts as per Wang *et al.* (2007). Asexual animals were maintained at 21°C as described by Sánchez Alvarado *et al.* (2002) with modifications to the Montjuïc salts formula as per Pearson and Gurley (http://lab.research.sickkids.ca/pearson/wp-content/uploads/sites/54/2015/10/Planarian_careNfeedingNliverprep_Pearson.pdf).

Both strains are maintained on a weekly to semiweekly diet of calf liver and starved for a week prior to experimentation.

Identification and cloning of *S. mediterranea* TTBK homologues
Planarian homologues of human TTBK1 and TTBK2 protein sequences were identified in a reference transcriptome assembly including cDNA and RNAseq reads from the sexual strain of *S. mediterranea* (Rouhana *et al.*, 2012) using the TBLASTN function in BlastStation Local64 (TM Software, Arcadia, CA). Orthologous TTBK sequences were confirmed via reciprocal BLASTP searches of predicted planarian protein products and human reference protein sequences deposited in the NCBI (http://blast.ncbi.nlm.nih.gov). The existence of six planarian *TTBK* orthologues in *S. mediterranea* was verified in genomic sequences from Robb *et al.* (2008) and Grohme *et al.* (2018) by BLASTN searches in SmedGD (Robb *et al.*, 2015) and PlanMine (Brandl *et al.*, 2016). Amplicons containing kinase domain sequence corresponding to each of the six *TTBK* paralogues as well as casein kinase homologues were amplified from sexual *S. mediterranea* total cDNA using the following primers: *Smed-TTBK-a*, 5'-ACAAGGAAGA-GAGCATTCTTGTAGA-3' and 5'-ATCAGGAGAATCAAAGTATGT-GAGG-3'; *Smed-TTBK-b*, 5'-GGAAGTAGCAGTGCTGAAAAGA TTA-3' and 5'-CAACTACTGAAATTTATGCCTCGC-3'; *Smed-TTBK-c*, 5'-GCTAAGTGCTCAAATCCTTCAATC-3' and 5'-ACTCA TCGGAACTTATTCCTTTACG-3'; *Smed-TTBK-d*, 5'-CTTCAACT-CAAGAACCTGATTTAGC-3' and 5'-TATCTAACTGTTCCACGA-AAACCAG-3'; *Smed-TTBK-e*, 5'-TTAATAGAGCCAGGTCACCT-CATTA-3' and 5'-CATATCTAACTGTTCCACGAAAACC-3'; *Smed-TTBK-f*, 5'-GTAATGTCTCTCCAAGGGAAAAACT-3' and 5'-CCA-GTATTTGTTTAAACTCCAGAGG-3'; *Smed-CSNK1-a*, 5'-AAGT-CAATAAAAGTCGTGCTAGTGG-3' and 5'-CCCAAAATAACTTAC-GCATGTAGTC-3'; *Smed-CSNK1-e*, 5'-GAAGAAAATTGGCTCA-GGTACTTTC-3' and 5'-ACTTTGCTGTTCCTGTTAAGTTCTG-3'. Amplicons were ligated into pGEM-T as per the manufacturer's protocol (Promega, Madison, WI), verified by Sanger sequencing, and sequence records were deposited in GenBank (Accession No. MH367867-MH367874). GeneArt Strings DNA fragments (ThermoFisher, Waltham, MA) containing sequences that correspond to different regions of *Smed-TTBK- a*, *-b*, *-c*, *-d*, *-e*, and *-f* cDNA (Supplemental Figure S7) than the ones cloned in pGEM-T were used to verify results obtained from RNAi and in situ hybridization. Sequences corresponding to *S. mediterranea* homologues of the MAP2/Tau family transcriptomes were also synthesized as GeneArt Strings DNA fragments (Supplemental Figure S7) and used as templates for downstream applications. Firefly *luciferase* and *PC2* (Collins *et al.*, 2010) partial cDNA sequences were included as negative and positive controls, respectively.

Whole-mount in situ hybridization
Sexual planarians of 1.0–1.5 cm length, or asexual planarians of 0.3–0.6 cm length, were processed for in situ hybridization as described by King and Newmark (2013), with modifications for sexual planarians as described below. Briefly, samples were rinsed with husbandry media and killed by incubating placed horizontally for 10 min on a rocking platform in a phosphate-buffered saline (PBS) solution containing 7.5% N-acetyl cysteine (NAC). The NAC solution was replaced with PBS containing 0.3% Triton-X (PBSTx) and 4% formaldehyde, and samples were incubated for 1 h for fixation. Then, samples were gradually dehydrated into methanol, placed overnight at –20°C, gradually

rehydrated into PBSTx, bleached in a formamide-based hydrogen peroxide solution under fluorescent light for 1.5–2 h, rinsed in PBSTx, and treated for 12 min with 10 µg/ml Proteinase K (Roche, Mannheim, Germany) in a PBSTx solution containing 0.1% SDS and postfixed for 10 min in PBSTx containing 4% formaldehyde. Subsequent steps for incubation with digoxigenin-11-UTP (DIG; Roche, Mannheim, Germany)-labeled riboprobes, posthybridization washes, incubation with anti-DIG antibodies, and washes in TNTx (100 mM Tris, pH 7.5, 150 mM NaCl, 0.3% Triton-X) after the antibody-binding step were performed as per King and Newmark (2013). Samples subjected to colorimetric detection of riboprobe hybridization were incubated with anti–DIG-AP (1:4000 dilution; Roche, Mannheim, Germany, Catalog No. 11093274910), developed as per Pearson *et al.* (2009), mounted on microscope slides in 4:1 glycerol:PBS (vol/vol), and imaged using a Zeiss V.16 SteREO microscope equipped with a Canon EOS Rebel T3 camera. For FISH analyses, samples were incubated overnight in anti–DIG-POD (1:1000 dilution; Roche, Mannheim, Germany, Catalog No. 11207733910), developed using FAM tyramide solution as per (King and Newmark, 2013), cleared and mounted in 4:1 glycerol/PBSTx, and imaged using a Nikon C2+ confocal microscope equipped with NIS Elements C software.

Whole-mount immunofluorescence, lectin, and DAPI staining

Analyses using anti-AcTub (1:500 dilution; clone 6-11B-1, Sigma Aldrich, St. Louis, MO) were performed on whole-mount asexual planarians fixed by HCl and paraformaldehyde treatment as per Ross *et al.* (2015). For whole-mount immunofluorescence using anti–α-tubulin (1:1000 dilution; clone B-5-1-2, Sigma Aldrich, St. Louis, MO), ConA (1:1000 dilution; Vector Laboratories, Burlingame, CA, Catalog No. FL-1001), and/or DAPI (5µg/ml; Acros Organics, Morris, NJ), planarian samples were prepared through NAC, formaldehyde, and bleaching treatments as described for whole-mount in situ hybridization (above). Steps for methanol dehydration and overnight storage at –20°C usually performed for in situ hybridization were omitted. For DAPI staining alone, bleached samples were washed twice with PBSTx, incubated overnight in a PBSTx solution containing DAPI, washed six times with PBSTx, mounted on slides, and imaged under UV light using a Zeiss V.16 SteREO microscope equipped with a Canon EOS Rebel T3 camera (low magnification) or a Nikon C2+ confocal microscope equipped with NIS Elements C software (20× objective or 60× oil immersion objective). For visualization of cilia of the planarian epidermis, bleached samples were incubated for2 h in Blocking solution (0.5% fish gelatin; 1% bovine serum albumin in PBSTx; Forsthoefel et al., 2014), followed by overnight incubation at 4°C in blocking solution supplemented with monoclonal anti–α-tubulin antibody or anti-AcTub. After overnight incubation, the samples were rinsed twice with PBSTx and washed six additional times for 15 min each with PBSTx, incubated for 3 h at room temperature or overnight at 4°C with secondary antibody in blocking solution (1:400 dilution of goat-anti-mouse immunoglobulin G (IgG) Alexa Fluor 488–conjugated [Cat. No. A11029, ThermoFisher, Waltham, MA] or goat-anti-mouse IgG Alexa Fluor 633 [Cat. No. A21050, ThermoFisher, Waltham, MA]), washed with PBSTx, stained with DAPI (as above), washed, and mounted on slides in 4:1 glycerol/PBS (vol/vol). Epithelial cells visualized by ConA were stained by extending the incubation with DAPI overnight at 4°C and including 5µg/ml Fluorescein–conjugated ConA lectin during the incubation. Samples were mounted with their dorsal end adjacent to the slide cover for analysis of testes, or with their ventral side

facing the slide cover for analysis of ventral epithelial cells, and imaged on a Nikon C2+ confocal microscope equipped with NIS Elements C software (60× oil immersion).

Preparation of riboprobes and dsRNA by in vitro transcription

Amplicons containing *Smed-TTBK* paralogue, *PC2*, or *luciferase* partial cDNA sequence, upstream of an antisense SP6 promoter sequence, and flanked by T7 promoters were synthesized from pGEM-T constructs using the following primers: 5′-GCGCGAATTAACCCTCACTAAAGTAATACGACTCACTATAGGGCGAATTGG-3′; 5′-CGCG-CGCTAATACGACTCACTATAGGGCGCCAAGCTATTTAGGTGA-CACTATAG-3′. Amplicons containing an antisense T3 promoter, flanking T7 promoters, and partial cDNA sequence corresponding to *Smed-TTBK* cDNAs (outside of the kinase domain), *Smed-MAPT-L* paralogues, *PC2*, or *luciferase* were generated by PCR from GeneArt Strings DNA templates (ThermoFisher, Waltham, MA; Supplemental Figure S7) using the following primers: 5′-GAATTTAATACGACTCACTATAGGGGCGATTTAGGTGACACTATAGAAGAGAAC-3′; 5′-GAATT-TAATACGACTCACTATAGGGCGAATTAACCCTCACTA-AAGGGAAC-3′ as in Counts *et al.* (2017). Amplicons were purified using DNA Clean & Concentrator-5 columns (Zymo Research, Irvine, CA), eluted in 20 µl of nuclease-free water, and used as templates for in vitro transcription. For RNAi, dsRNA was synthesized using T7 RNA Polymerase as per Rouhana *et al.* (2013) from the same templates generated by PCR from pGEM-T constructs and GeneArt Strings as described above. DIG-11-UTP and Fluorescin-12-UTP (Sigma Aldrich, St. Louis, MO)-labeled riboprobes were synthesized as per King and Newmark (2013) using either SP6 RNA Polymerase (amplicons generated from pGEM-T cDNA constructs) or T3 RNA Polymerase (GeneArt Strings amplicons). DIG-labeled riboprobes were precipitated using lithium chloride after DNase treatment and resuspended in hybridization buffer.

RNAi

RNAi was performed as per Rouhana *et al.* (2013). Briefly, groups of five planarians were fed to satiation with liver solution containing gene-specific dsRNA at a concentration of ~100 ng/µl every 3–4 d for 3 or 4 wk. dsRNA with sequence corresponding to firefly *luciferase*, which does not disturb planarian somatic or reproductive physiology, was used as a negative control. One week after their final dsRNA feeding, planarians were subjected to behavioral analyses in response to light stimuli, amputated for regeneration assays, or fixed for anatomical analysis. For combinatorial gene knockdown, liver was supplemented with 125–150 ng/µl of dsRNA composed of equal amounts of all six *Smed-TTBK* paralogues. For mixtures of dsRNA targeting less than six paralogues, the amount of dsRNA for each gene was kept constant (one-sixth) and brought up to a total dsRNA concentration of 125–150 ng/µl with *luciferase* dsRNA.

Light-response assay

On completion of RNAi treatment groups of five planarians subjected to either *luciferase* or *Smed-TTBK-d* knockdown were collected in a 50-ml conical tube, washed with 5 ml of 0.75× Montjuïc salts, and decanted into a 150 × 15-mm Petri dish filled with 25 ml 0.75× Montjuïc salts. White light from a Fiber-Lite high intensity illuminator (Series 180, Dolon-Jenner Industries, Boxborough, MA) at the maximum strength was directed to the most proximal region of the plate (see Figure 6, C and D) from a vertical distance of 20 cm. Planarians were decanted in the illuminated region and migration to less illuminated regions of the Petri dish were recorded for 3 min for

both *luciferase(RNAi)* and *Smed-TTBK-d(RNAi)* groups. At the end of 2 min, the experiment was conducted again with reciprocal placement of planarian groups in Petri dishes. Time spent by each planarian in each of the five positions of the plate was averaged for four runs using two groups of biological replicates. Standard deviation from the mean and two-tailed Student's *t* test were calculated for statistical analysis.

Live imaging of motile cilia and TEM

Asexual planarians of 1–3 mm length were subjected to 3 wk of *luciferase* or *Smed-TTBK-d* RNAi and either mounted on glass slides for live imaging of cilia or fixed overnight at room temperature in a PBS solution supplemented with glutaraldehyde. Fixed samples were submitted to the Campus Microscopy and Imaging Facility at The Ohio State University for TEM processing and analysis. For live imaging of cilia, planarians were mounted in modified Montjuïc salts (see *Planarian cultures* above) on a glass microscope slide adhered to a perforated sheet of Parafilm and capped with a slide cover as per Rompolas *et al.* (2013). Movement of cilia in the peripheral epithelium of *luciferase(RNAi)* and *Smed-TTBK-d(RNAi)* were imaged by phase contrast under oil immersion using a 100× objective on a Nikon Eclipse E200 microscope and recorded with an Apple iPhone X mounted on a universal cell phone photography adapter (Amazon Standard Identification Number B07BC8SBR7; Gosky Optics, China). Videos were cropped and converted to .mov files using Apple iMovie software.

REFERENCES
Almuedo-Castillo M, Sureda-Gomez M, Adell T (2012). Wnt signaling in planarians: new answers to old questions. Int J Dev Biol 56, 53–65.

Ashman JB, Hall ES, Eveleth J, Boekelheide K (1992). Tau, the neuronal heat-stable microtubule-associated protein, is also present in the cross-linked microtubule network of the testicular spermatid manchette. Biol Reprod 46, 120–129.

Azimzadeh J, Basquin C (2016). Basal bodies across eukaryotes series: basal bodies in the freshwater planarian Schmidtea mediterranea. Cilia 5, 15.

Azimzadeh J, Wong ML, Downhour DM, Sánchez Alvarado A, Marshall WF (2012). Centrosome loss in the evolution of planarians. Science 335, 461–463.

Badano JL, Mitsuma N, Beales PL, Katsanis N (2006). The ciliopathies: an emerging class of human genetic disorders. Annu Rev Genomics Hum Genet 7, 125–148.

Basquin C, Orfila AM, Azimzadeh J (2015). The planarian Schmidtea mediterranea as a model for studying motile cilia and multi-ciliated cells. Methods Cell Biol 127, 243–262.

Bauer P, Stevanin G, Beetz C, Synofzik M, Schmitz-Hubsch T, Wullner U, Berthier E, Ollagnon-Roman E, Riess O, Forlani S, et al. (2010). Spinocerebellar ataxia type 11 (SCA11) is an uncommon cause of dominant ataxia among French and German kindreds. J Neurol Neurosurg Psychiatry 81, 1229–1232.

Bouskila M, Esoof N, Gay L, Fang EH, Deak M, Begley MJ, Cantley LC, Prescott A, Storey KG, Alessi DR (2011). TTBK2 kinase substrate specificity and the impact of spinocerebellar-ataxia-causing mutations on expression, activity, localization and development. Biochem J 437, 157–167.

Bowie E, Norris R, Anderson KV, Goetz SC (2018). Spinocerebellar ataxia type 11-associated alleles of Ttbk2 dominantly interfere with ciliogenesis and cilium stability. PLoS Genet 14, e1007844.

Brandl H, Moon H, Vila-Farre M, Liu SY, Henry I, Rink JC (2016). PlanMine—a mineable resource of planarian biology and biodiversity. Nucleic Acids Res 44, D764–D773.

Cajanek L, Nigg EA (2014). Cep164 triggers ciliogenesis by recruiting Tau tubulin kinase 2 to the mother centriole. Proc Natl Acad Sci USA 111, E2841–E2850.

Chong T, Collins JJ 3rd, Brubacher JL, Zarkower D, Newmark PA (2013). A sex-specific transcription factor controls male identity in a simultaneous hermaphrodite. Nat Commun 4, 1814.

Chong T, Stary JM, Wang Y, Newmark PA (2011). Molecular markers to characterize the hermaphroditic reproductive system of the planarian Schmidtea mediterranea. BMC Dev Biol 11, 69.

Collins JJ 3rd, Hou X, Romanova EV, Lambrus BG, Miller CM, Saberi A, Sweedler JV, Newmark PA (2010). Genome-wide analyses reveal a role for peptide hormones in planarian germline development. PLoS Biol 8, e1000509.

Counts JT, Hester TM, Rouhana L (2017). Genetic expansion of chaperonin-containing TCP-1 (CCT/TRiC) complex subunits yields testis-specific isoforms required for spermatogenesis in planarian flatworms. Mol Reprod Dev 84, 1271–1284.

Davies EL, Lei K, Seidel CW, Kroesen AE, McKinney SA, Guo L, Robb SM, Ross EJ, Gotting K, Sanchez Alvarado A (2017). Embryonic origin of adult stem cells required for tissue homeostasis and regeneration. Elife 6, e21052.

Dereeper A, Guignon V, Blanc G, Audic S, Buffet S, Chevenet F, Dufayard JF, Guindon S, Lefort V, Lescot M, et al. (2008). Phylogeny.fr: robust phylogenetic analysis for the non-specialist. Nucleic Acids Res 36, W465–W469.

Elliott SA, Sánchez Alvarado A (2013). The history and enduring contributions of planarians to the study of animal regeneration. Wiley Interdiscip Rev Dev Biol 2, 301–326.

Fagerberg L, Hallstrom BM, Oksvold P, Kampf C, Djureinovic D, Odeberg J, Habuka M, Tahmasebpoor S, Danielsson A, Edlund K, et al. (2014). Analysis of the human tissue-specific expression by genome-wide integration of transcriptomics and antibody-based proteomics. Mol Cell Proteomics 13, 397–406.

Fincher CT, Wurtzel O, de Hoog T, Kravarik KM, Reddien PW (2018). Cell type transcriptome atlas for the planarian Schmidtea mediterranea. Science 360, eaaq1736.

Flotow H, Graves PR, Wang AQ, Fiol CJ, Roeske RW, Roach PJ (1990). Phosphate groups as substrate determinants for casein kinase I action. J Biol Chem 265, 14264–14269.

Flotow H, Roach PJ (1989). Synergistic phosphorylation of rabbit muscle glycogen synthase by cyclic AMP-dependent protein kinase and casein kinase I. Implications for hormonal regulation of glycogen synthase. J Biol Chem 264, 9126–9128.

Forsthoefel DJ, Waters FA, Newmark PA (2014). Generation of cell type-specific monoclonal antibodies for the planarian and optimization of sample processing for immunolabeling. BMC Dev Biol 14, 45.

Glazer AM, Wilkinson AW, Backer CB, Lapan SW, Gutzman JH, Cheeseman IM, Reddien PW (2010). The Zn finger protein Iguana impacts Hedgehog signaling by promoting ciliogenesis. Dev Biol 337, 148–156.

Goetz SC, Liem KF Jr, Anderson KV (2012). The spinocerebellar ataxia-associated gene Tau tubulin kinase 2 controls the initiation of ciliogenesis. Cell 151, 847–858.

Grohme MA, Schloissnig S, Rozanski A, Pippel M, Young GR, Winkler S, Brandl H, Henry I, Dahl A, Powell S, et al. (2018). The genome of Schmidtea mediterranea and the evolution of core cellular mechanisms. Nature 554, 56–61.

Gu Y, Oyama F, Ihara Y (1996). Tau is widely expressed in rat tissues. J Neurochem 67, 1235–1244.

Hanks SK, Hunter T (1995). Protein kinases 6. The eukaryotic protein kinase superfamily: kinase (catalytic) domain structure and classification. FASEB J 9, 576–596.

Higuchi S, Hayashi T, Tarui H, Nishimura O, Nishimura K, Shibata N, Sakamoto H, Agata K (2008). Expression and functional analysis of musashi-like genes in planarian CNS regeneration. Mech Dev 125, 631–645.

Houlden H, Johnson J, Gardner-Thorpe C, Lashley T, Hernandez D, Worth P, Singleton AB, Hilton DA, Holton J, Revesz T, et al. (2007). Mutations in

TTBK2, encoding a kinase implicated in tau phosphorylation, segregate with spinocerebellar ataxia type 11. Nat Genet 39, 1434–1436.

Ikezu S, Ikezu T (2014). Tau-tubulin kinase. Front Mol Neurosci 7, 33.

Inoue H, Hiradate Y, Shirakata Y, Kanai K, Kosaka K, Gotoh A, Fukuda Y, Nakai Y, Uchida T, Sato E, Tanemura K (2014). Site-specific phosphorylation of Tau protein is associated with deacetylation of microtubules in mouse spermatogenic cells during meiosis. FEBS Lett 588, 2003–2008.

Inoue T, Hoshino H, Yamashita T, Shimoyama S, Agata K (2015). Planarian shows decision-making behavior in response to multiple stimuli by integrative brain function. Zool Lett 1, 7.

Inoue T, Kumamoto H, Okamoto K, Umesono Y, Sakai M, Sánchez Alvarado A, Agata K (2004). Morphological and functional recovery of the planarian photosensing system during head regeneration. Zoolog Sci 21, 275–283.

Ishii S (1980). The ultrastructure of the protonephridial tubules of the freshwater planarian Bdellocephala brunnea. Cell Tissue Res 206, 451–458.

Kiefer SE, Chang CJ, Kimura SR, Gao M, Xie D, Zhang Y, Zhang G, Gill MB, Mastalerz H, Thompson LA, et al. (2014). The structure of human tau-tubulin kinase 1 both in the apo form and in complex with an inhibitor. Acta Crystallogr F Struct Biol Commun 70, 173–181.

King RS, Newmark PA (2013). In situ hybridization protocol for enhanced detection of gene expression in the planarian Schmidtea mediterranea. BMC Dev Biol 13, 8.

King SM, Patel-King RS (2016). Planaria as a model system for the analysis of ciliary assembly and motility. Methods Mol Biol 1454, 245–254.

Lalmansingh AS, Urekar CJ, Reddi PP (2011). TDP-43 is a transcriptional repressor: the testis-specific mouse acrv1 gene is a TDP-43 target in vivo. J Biol Chem 286, 10970–10982.

Lee JE, Gleeson JG (2011). Cilia in the nervous system: linking cilia function and neurodevelopmental disorders. Curr Opin Neurol 24, 98–105.

Lehti MS, Kotaja N, Sironen A (2013). KIF3A is essential for sperm tail formation and manchette function. Mol Cell Endocrinol 377, 44–55.

Liachko NF, McMillan PJ, Strovas TJ, Loomis E, Greenup L, Murrell JR, Ghetti B, Raskind MA, Montine TJ, Bird TD, et al. (2014). The tau tubulin kinases TTBK1/2 promote accumulation of pathological TDP-43. PLoS Genet 10, e1004803.

Liu SY, Selck C, Friedrich B, Lutz R, Vila-Farre M, Dahl A, Brandl H, Lakshmanaperumal N, Henry I, Rink JC (2013). Reactivating head regrowth in a regeneration-deficient planarian species. Nature 500, 81–84.

Loveland KL, Hayes TM, Meinhardt A, Zlatic KS, Parvinen M, de Kretser DM, McFarlane JR (1996). Microtubule-associated protein-2 in the rat testis: a novel site of expression. Biol Reprod 54, 896–904.

Loveland KL, Herszfeld D, Chu B, Rames E, Christy E, Briggs LJ, Shakri R, de Kretser DM, Jans DA (1999). Novel low molecular weight microtubule-associated protein-2 isoforms contain a functional nuclear localization sequence. J Biol Chem 274, 19261–19268.

McKanna JA (1968a). Fine structure of the protonephridial system in Planaria. I. Flame cells. Z Zellforsch Mikrosk Anat 92, 509–523.

McKanna JA (1968b). Fine structure of the protonephridial system in Planaria. II. Ductules, collecting ducts, and osmoregulatory cells. Z Zellforsch Mikrosk Anat 92, 524–535.

Nakielny S, Campbell DG, Cohen P (1991). The molecular mechanism by which adrenalin inhibits glycogen synthesis. Eur J Biochem 199, 713–722.

Newmark PA, Reddien PW, Cebria F, Sánchez Alvarado A (2003). Ingestion of bacterially expressed double-stranded RNA inhibits gene expression in planarians. Proc Natl Acad Sci USA 100 (suppl 1), 11861–11865.

Newmark PA, Sánchez Alvarado A (2000). Bromodeoxyuridine specifically labels the regenerative stem cells of planarians. Dev Biol 220, 142–153.

Newmark PA, Sánchez Alvarado A (2002). Not your father's planarian: a classic model enters the era of functional genomics. Nat Rev Genet 3, 210–219.

Newmark PA, Wang Y, Chong T (2008). Germ cell specification and regeneration in planarians. Cold Spring Harb Symp Quant Biol 73, 573–581.

Oda T, Chiba S, Nagai T, Mizuno K (2014). Binding to Cep164, but not EB1, is essential for centriolar localization of TTBK2 and its function in ciliogenesis. Genes Cells 19, 927–940.

Papatheodorou I, Fonseca NA, Keays M, Tang YA, Barrera E, Bazant W, Burke M, Fullgrabe A, Fuentes AM, George N, et al. (2018). Expression Atlas: gene and protein expression across multiple studies and organisms. Nucleic Acids Res 46, D246–D251.

Pearson BJ, Eisenhoffer GT, Gurley KA, Rink JC, Miller DE, Sánchez Alvarado A (2009). Formaldehyde-based whole-mount in situ hybridization method for planarians. Dev Dyn 238, 443–450.

Plass M, Solana J, Wolf FA, Ayoub S, Misios A, Glažar P, Obermayer B, Theis FJ, Kocks C, Rajewsky N (2018). Cell type atlas and lineage tree of a whole complex animal by single-cell transcriptomics. Science 360, eaaq1723.

Qi H, Yao C, Cai W, Girton J, Johansen KM, Johansen J (2009). Asator, a tau-tubulin kinase homolog in Drosophila localizes to the mitotic spindle. Dev Dyn 238, 3248–3256.

Reddien PW, Bermange AL, Murfitt KJ, Jennings JR, Sánchez Alvarado A (2005). Identification of genes needed for regeneration, stem cell function, and tissue homeostasis by systematic gene perturbation in planaria. Dev Cell 8, 635–649.

Reiter JF, Leroux MR (2017). Genes and molecular pathways underpinning ciliopathies. Nat Rev Mol Cell Biol 18, 533–547.

Rink JC (2013). Stem cell systems and regeneration in planaria. Dev Genes Evol 223, 67–84.

Rink JC, Gurley KA, Elliott SA, Sánchez Alvarado A (2009). Planarian Hh signaling regulates regeneration polarity and links Hh pathway evolution to cilia. Science 326, 1406–1410.

Rink JC, Vu HT, Sánchez Alvarado A (2011). The maintenance and regeneration of the planarian excretory system are regulated by EGFR signaling. Development 138, 3769–3780.

Robb SM, Gotting K, Ross E, Sánchez Alvarado A (2015). SmedGD 2.0: The Schmidtea mediterranea genome database. Genesis 53, 535–546.

Robb SM, Ross E, Sánchez Alvarado A (2008). SmedGD: the Schmidtea mediterranea genome database. Nucleic Acids Res 36, D599–D606.

Rompolas P, Azimzadeh J, Marshall WF, King SM (2013). Analysis of ciliary assembly and function in planaria. Methods Enzymol 525, 245–264.

Rompolas P, Patel-King RS, King SM (2009). Schmidtea mediterranea: a model system for analysis of motile cilia. Methods Cell Biol 93, 81–98.

Rompolas P, Patel-King RS, King SM (2010). An outer arm Dynein conformational switch is required for metachronal synchrony of motile cilia in planaria. Mol Biol Cell 21, 3669–3679.

Ross KG, Molinaro AM, Romero C, Dockter B, Cable KL, Gonzalez K, Zhang S, Collins ES, Pearson BJ, Zayas RM (2018). SoxB1 activity regulates sensory neuron regeneration, maintenance, and function in planarians. Dev Cell 47, 331–347.e335.

Ross KG, Omuro KC, Taylor MR, Munday RK, Hubert A, King RS, Zayas RM (2015). Novel monoclonal antibodies to study tissue regeneration in planarians. BMC Dev Biol 15, 2.

Rouhana L, Tasaki J, Saberi A, Newmark PA (2017). Genetic dissection of the planarian reproductive system through characterization of Schmidtea mediterranea CPEB homologs. Dev Biol 426, 43–55.

Rouhana L, Vieira AP, Roberts-Galbraith RH, Newmark PA (2012). PRMT5 and the role of symmetrical dimethylarginine in chromatoid bodies of planarian stem cells. Development 139, 1083–1094.

Rouhana L, Weiss JA, Forsthoefel DJ, Lee H, King RS, Inoue T, Shibata N, Agata K, Newmark PA (2013). RNA interference by feeding in vitro-synthesized double-stranded RNA to planarians: methodology and dynamics. Dev Dyn 242, 718–730.

Saló E, Baguñà J (1985). Cell movement in intact and regenerating planarians. Quantitation using chromosomal, nuclear and cytoplasmic markers. J Embryol Exp Morphol 89, 57–70.

Saló E, Baguñà J (1989). Regeneration and pattern-formation in planarians .2. Local origin and role of cell movements in blastema formation. Development 107, 69–76.

Samora CP, Mogessie B, Conway L, Ross JL, Straube A, McAinsh AD (2011). MAP4 and CLASP1 operate as a safety mechanism to maintain a stable spindle position in mitosis. Nat Cell Biol 13, 1040–1050.

Sánchez Alvarado A, Newmark PA (1999). Double-stranded RNA specifically disrupts gene expression during planarian regeneration. Proc Natl Acad Sci 96, 5049–5054.

Sánchez Alvarado A, Newmark PA, Robb SM, Juste R (2002). The Schmidtea mediterranea database as a molecular resource for studying platyhelminthes, stem cells and regeneration. Development 129, 5659–5665.

Sato S, Cerny RL, Buescher JL, Ikezu T (2006). Tau-tubulin kinase 1 (TTBK1), a neuron-specific tau kinase candidate, is involved in tau phosphorylation and aggregation. J Neurochem 98, 1573–1584.

Sato S, Xu J, Okuyama S, Martinez LB, Walsh SM, Jacobsen MT, Swan RJ, Schlautman JD, Ciborowski P, Ikezu T (2008). Spatial learning impairment, enhanced CDK5/p35 activity, and downregulation of NMDA receptor expression in transgenic mice expressing tau-tubulin kinase 1. J Neurosci 28, 14511–14521.

Scimone ML, Srivastava M, Bell GW, Reddien PW (2011). A regulatory program for excretory system regeneration in planarians. Development 138, 4387–4398.

Shibata N, Rouhana L, Agata K (2010). Cellular and molecular dissection of pluripotent adult somatic stem cells in planarians. Dev Growth Differ 52, 27–41.

Sigala J, Jumeau F, Caillet-Boudin ML, Sergeant N, Ballot C, Rigot JM, Marcelli F, Tardivel M, Buee L, Mitchell V (2014). Immunodetection of Tau microtubule-associated protein in human sperm and testis. Asian J Androl 16, 927–928.

Steiner JK, Tasaki J, Rouhana L (2016). Germline defects caused by Smed-boule RNA-interference reveal that egg capsule deposition occurs independently of fertilization, ovulation, mating, or the presence of gametes in planarian flatworms. PLoS Genet 12, e1006030.

Sundermann F, Fernandez MP, Morgan RO (2016). An evolutionary roadmap to the microtubule-associated protein MAP Tau. BMC Genomics 17, 264.

Takahashi M, Tomizawa K, Sato K, Ohtake A, Omori A (1995). A novel tau-tubulin kinase from bovine brain. FEBS Lett 372, 59–64.

Taylor LM, McMillan PJ, Liachko NF, Strovas TJ, Ghetti B, Bird TD, Keene CD, Kraemer BC (2018). Pathological phosphorylation of tau and TDP-43 by TTBK1 and TTBK2 drives neurodegeneration. Mol Neurodegener 13, 7.

Thi-Kim Vu H, Rink JC, McKinney SA, McClain M, Lakshmanaperumal N, Alexander R, Sánchez Alvarado A (2015). Stem cells and fluid flow drive cyst formation in an invertebrate excretory organ. Elife 4, e07405.

Tomizawa K, Omori A, Ohtake A, Sato K, Takahashi M (2001). Tau-tubulin kinase phosphorylates tau at Ser-208 and Ser-210, sites found in paired helical filament-tau. FEBS Lett 492, 221–227.

Vazquez-Higuera JL, Martinez-Garcia A, Sánchez-Juan P, Rodriguez-Rodriguez E, Mateo I, Pozueta A, Frank A, Valdivieso F, Berciano J, Bullido MJ, Combarros O (2011). Genetic variations in tau-tubulin kinase-1 are linked to Alzheimer's disease in a Spanish case-control cohort. Neurobiol Aging 32, 550 e555–e559.

Vij S, Rink JC, Ho HK, Babu D, Eitel M, Narasimhan V, Tiku V, Westbrook J, Schierwater B, Roy S (2012). Evolutionarily ancient association of the FoxJ1 transcription factor with the motile ciliogenic program. PLoS Genet 8, e1003019.

Wagner DE, Wang IE, Reddien PW (2011). Clonogenic neoblasts are pluripotent adult stem cells that underlie planarian regeneration. Science 332, 811–816.

Wang Y, Stary JM, Wilhelm JE, Newmark PA (2010). A functional genomic screen in planarians identifies novel regulators of germ cell development. Genes Dev 24, 2081–2092.

Wang Y, Zayas RM, Guo T, Newmark PA (2007). nanos function is essential for development and regeneration of planarian germ cells. Proc Natl Acad Sci USA 104, 5901–5906.

Waters AM, Beales PL (2011). Ciliopathies: an expanding disease spectrum. Pediatr Nephrol 26, 1039–1056.

Wurtzel O, Cote LE, Poirier A, Satija R, Regev A, Reddien PW (2015). A generic and cell-type-specific wound response precedes regeneration in planarians. Dev Cell 35, 632–645.

Yu NN, Yu JT, Xiao JT, Zhang HW, Lu RC, Jiang H, Xing ZH, Tan L (2011). Tau-tubulin kinase-1 gene variants are associated with Alzheimer's disease in Han Chinese. Neurosci Lett 491, 83–86.

Zayas RM, Cebria F, Guo T, Feng J, Newmark PA (2010). The use of lectins as markers for differentiated secretory cells in planarians. Dev Dyn 239, 2888–2897.

Zayas RM, Hernandez A, Habermann B, Wang Y, Stary JM, Newmark PA (2005). The planarian Schmidtea mediterranea as a model for epigenetic germ cell specification: analysis of ESTs from the hermaphroditic strain. Proc Natl Acad Sci USA 102, 18491–18496.